Title: Chemokine signaling links cell cycle progression and cilia formation for left-right symmetry breaking

Authors: Jingwen Liu[1#], Chengke Zhu[4#], Guozhu Ning[2], Liping Yang[2], Yu Cao[1], Sizhou Huang[3]*, Qiang Wang[1, 2, 5, 6] *

Affiliations: [1]School of Life Sciences, University of Science and Technology of China, Anhui, Hefei 230026, China; [2]State Key Laboratory of Membrane Biology, Institute of Zoology, University of Chinese Academy of Sciences, Chinese Academy of Sciences, Beijing 100101, China; [3]Development and Regeneration Key Laboratory of Sichuan Province, Department of Anatomy and Histology and Embryology, Chengdu Medical College, Chengdu 610083, China; [4] Key Laboratary of Freshwater Fish Reproduction and Development, Ministry of Education, Key Laboratory of Aquatics Science of Chongqing, College of Animal Science in Rongchang Campus, Southwest University, Chongqing 402460, China; [5]Institute for Stem Cell and Regeneration, Chinese Academy of Sciences, Beijing 100101, China; [6] Lead Contact.

# These authors share first authorship on this work.

*Correspondence may be addressed to: Tel: 86-28-62739298; Fax: 86-28-62739298; E-mail: huangyuy1027@cmc.edu.cn

*Correspondence may be addressed to: Tel: 86-10-64807895; Fax: 86-10-64807895; E-mail: qiangwang@ioz.ac.cn

Running title: Cxcr4a guides cell proliferation and ciliogenesis.

Abstract

Zebrafish dorsal forerunner cells (DFCs) undergo vigorous proliferation during epiboly and then exit cell cycle to generate Kupffer's vesicle (KV), a ciliated organ necessary for establishing left-right (L-R) asymmetry. DFC proliferation defects are often accompanied by impaired cilia elongation in KV, but the functional and molecular interaction between cell-cycle progression and cilia formation remains unknown. Here we show that chemokine receptor Cxcr4a is required for L-R laterality by controlling DFC proliferation and KV ciliogenesis. Functional analysis revealed that Cxcr4a accelerates G1/S transition in DFCs and stabilizes Foxj1a, a master regulator of motile cilia, by stimulating Cyclin D1 expression through ERK1/2 signaling. Mechanistically, Cyclin D1-CDK4/6 drives G1/S transition during DFC proliferation and phosphorylates Foxj1a, thereby disrupting its association with Psmd4b, a 19S regulatory subunit. This prevents the ubiquitin-independent proteasomal degradation of Foxj1a. Our study uncovers a role for Cxcr4 signaling in L-R patterning and provides fundamental insights into the molecular linkage between cell-cycle progression and ciliogenesis.

Keywords: left-right asymmetry, *cxcr4a*, G1/S transition, ciliogenesis, Cyclin D1-CDK4/6, Foxj1a, Psmd4b, ubiquitin-independent proteasomal degradation.

Author summary

During the organogenesis of zebrafish L-R organizer named KV, DFCs proliferate rapidly during epiboly and then exit the cell cycle to differentiate into ciliated epithelial KV cells. Cell cycle defects in DFCs are often accompanied by an alteration in KV cilia elongation. However, whether the cell cycle and cilia formation are mechanistically linked remains as an open question. In this study, we report that Cxcr4 signaling is required for DFC proliferation and KV ciliogenesis. We reveal that Cxcl12b/Cxcr4a signaling activates ERK1/2, which then promotes Cyclin D1 expression. Cyclin D1-CDK4/6 accelerates the G1/S transition in DFCs, while also facilitates cilia formation via stabilization of Foxj1a. Notably, Foxj1 undergoes proteasomal degradation via Ub-independent pathway during KV organogenesis. Our study further demonstrates that CDK4 phosphorylates and stabilizes Foxj1a by disrupting its association with Psmd4b, a 19S regulatory subunit. In summary, Cxcl12b/Cxcr4a chemokine signaling links cell cycle progression and cilia formation for L-R symmetry breaking via regulating Cyclin D1 expression.

Introduction

Vertebrates exhibit striking left-right (L-R) asymmetries in the structure and position of their cardiovascular and gastrointestinal systems. Initially, early embryos develop symmetrically along the prospective body midline. This embryonic symmetry is broken during somite stages when an asymmetric fluid flow is generated by motile cilia within the L-R organizer (LRO), a transient structure located at the posterior end of the notochord [1]. Specifically, in zebrafish, the ciliated LRO is referred to as Kupffer's vesicle (KV), which forms from dorsal forerunner cells (DFCs), a group of superficial cells in the organizer region of the gastrula [2,3]. It has been well established that the architecture of KV cells and asymmetric KV cilia generate a counter-clockwise nodal flow. This leads to the asymmetrical expression of early laterality genes, including *nodal-related southpaw* (*spaw*) and *pitx2c* in the left lateral plate mesoderm (LPM), and ultimately the establishment of L-R asymmetric patterning [4]. The origin of L-R asymmetry is conserved across many vertebrates, and defects in the establishment of these asymmetries can result in a broad spectrum of birth defects, often including congenital heart malformations [5,6].

The progression of cells through the G1 and S phases of the cell cycle is tightly controlled by the sequential activation of a family of serine-threonine kinases known as the cyclin-dependent kinases (CDKs). CDK4 and its homologous CDK6 are activated by D-type cyclins in early to mid-G1 phase, whereas CDK2 is activated by E- and A-type cyclins during late G1 and S phase, respectively [7]. Recent evidence indicates that cell cycle dynamics have emerged as a key regulator of stem cell fate

89 decisions [8-10]. Specifically, cyclin D proteins have been shown to activate CDK4/6,
90 which restricts the activity of Smad2/3 in late G1 phase and results in a switch from
91 endoderm to neuroectoderm potential in human pluripotent stem cells [11]. The G1
92 cyclin proteins together with their associated CDKs also play essential, direct roles in
93 the maintenance of cell stemness and in the regulation of cell fate specification in
94 mouse embryonic stem cells by phosphorylation and stabilization of the core
95 pluripotency factors, Nanog, Sox2, and Oct4 [12]. In addition, CDK4/CyclinD1
96 overexpression has been shown to prevent G1 lengthening and functions to inhibit
97 neurogenesis in mouse embryos [13]. In zebrafish, DFCs vigorously proliferate and
98 collectively migrate towards the vegetal pole during epiboly stages. They then cluster
99 and differentiate into polarized epithelial cells of KV [4,14,15]. Interestingly, DFC
100 proliferation defects are often accompanied by impaired cilia elongation in KV [16],
101 indicating a possible connection between cell-cycle events and KV cilia formation.
102 However, the underlying mechanism remains poorly understood.

103 Foxj1, a forkhead domain-containing transcription factor that is expressed in
104 various ciliated tissues, has been associated with motile cilia formation and L-R axis
105 development in mammals [17,18]. In zebrafish, two *foxj1* paralogs have been
106 identified, including *foxj1a* and *foxj1b* [19]. *foxj1a* has been shown to be highly
107 expressed in the DFCs toward the end of gastrulation and plays a primary role in KV
108 ciliogenesis, while *foxj1b* is expressed in the otic vesicle where it has been shown to
109 regulate motile cilia formation [19,20]. The expression level of *foxj1a* transcripts has
110 been shown to be regulated by the Hedgehog, Wnt/β-catenin and FGF signaling

pathways [19,21,22]. Lnx2b, a RING domain containing E3 ubiquitin (Ub) ligase, which is specifically expressed in the migratory DFCs and developing KV, plays a critical role in the establishment of L-R laterality. This indicates the involvement of protein ubiquitination in the determination of L-R asymmetry [23]. However, whether the function of Foxj1 protein in KV ciliogenesis is regulated by Ub modification remains unknown.

Chemokines are small (8-14 kDa) vertebrate-specific proteins that can be categorized into four subgroups according to the presence and position of conserved cysteine residues (C, CC, CXC, and CX3C) [24]. Among chemokines of the CXC class, the stromal cell-derived factor 1 (SDF-1/CXCL12) and its receptor CXCR4, which were first identified due to their primary role in leukocyte homing, have been implicated in the regulation of cell adhesion and migration during embryonic development [24-26]. Interestingly, in zebrafish, two Cxcl12 ligands and two Cxcr4 receptors were found to be expressed across a wide range of cell types and developmental stages, and were found to act as discrete pairs to direct cell migration [25]. Cxcl12a-Cxcr4b signaling controls processes such as the directional migration of primordial germ cells, the collective migration of the lateral line primordium, and the formation of the truck lymphatic network [27-29]. On the other hand, the Cxcl12b-Cxcr4a axis has been shown to play a role in endodermal morphogenesis, vascular system patterning, and the migration and prechondrogenic condensation of cranial neural crest cells [30-33]. It has been shown previously that *cxcr4a* and *cxcr4b* possess mutually exclusive expression patterns in the majority of cell lineages [34].

For example, *cxcr4a* but not *cxcr4b* is expressed in the primordium of KV [34]. While *cxcr4b* expression reveals an asymmetric pattern in habenular neurogenesis, the *cxcr4b* mutant *odysseus* displays no obvious phenotype in L-R epithalamic asymmetry [35]. These observations bring into question whether the signaling cascades initiated by Cxcl12b and Cxcr4a play a role in the establishment of L-R asymmetry.

Here, we provide evidence suggesting that the Cxcl12b-Cxcr4a axis is essential for L-R asymmetric development. *Cxcr4a*^{um20} mutants were found to exhibit poor DFC proliferation and abnormal KV cilia formation. Specifically, depletion of *cxcr4a* in DFCs was found to lead to a significant decrease in ERK1/2 signal activation, which was essential for the expression of *cyclin D1*. Subsequent biochemical and functional approaches demonstrated that Cyclin D1-CDK4/6 functions to accelerate the G1/S transition to promote DFC proliferation and stabilize Foxj1a for cilia formation. Mechanistically, CDK4 phosphorylates zFoxj1a at T102 and then disrupts its association with Psmd4b, which in turn prevents the ubiquitin-independent proteasomal degradation of Foxj1a protein. Therefore, Cxcl12b/Cxcr4a chemokine signaling links cell cycle progression and cilia formation for L-R symmetry breaking via regulating Cyclin D1 expression.

Results

Cxcl12b-Cxcr4a axis is required for L-R laterality

cxcr4a was previously found to be expressed in KV progenitors at the end of

gastrulation [34]. To address the detailed expression patterns of *cxcr4a*, whole mount *in situ* hybridization was carried out during early zebrafish embryogenesis. As shown in S1A Fig, *cxcr4a* expression was observed in endoderm cells and migrating DFCs throughout gastrulation. At early somite stages, concomitant with the onset of anterior neural plate expression, *cxcr4a* was also found to be activated in the developing KV cells besides the central lumen (S1B Fig). Therefore, we hypothesized that *cxcr4a* might play a critical role in KV organogenesis and L-R asymmetric patterning.

We then set out to test whether *cxcr4a* is required for L-R development in *cxcr4a*^{um20} embryos carrying loss-of-function mutations in *cxcr4a* gene, which lead to defects in lateral dorsal aorta formation (S1C Fig) [33]. In order to analyze the laterality information in homozygous *cxcr4a*^{um20} mutants, we examined cardiac development by WISH against cardiac myosin light chain 2 (*cmlc2*). At 48 hours post fertilization (hpf), the majority of wild-type embryos showed a heart tube looping to the right (D-loop) (Fig 1A and 1B). However, the heart localization became randomized in *cxcr4a*^{um20} mutants, of which 21% showed a “no-looping” or reversed “left-looping” heart (L-loop) (Fig 1A and 1B). In addition, in *cxcr4a*^{um20} embryos, the livers were also observed to be randomized in laterality as revealed by *hhex* expression (Fig 1C and 1D).

Because *cxcr4a* depletion would impair endoderm cell migration during gastrulation and cause bilateral duplication of endodermal organs such as the liver [30], we injected a previously validated morpholino that targets *cxcr4a* (*4a* MO) into embryonic yolk at the mid-blastula stage (256-cell stage) to specifically block *cxcr4a*

activity in DFC/KV cells, as demonstrated previously [36]. In comparison to injection with a standard control morpholino (cMO), injection of *4a* MO led to similar laterality abnormalities as observed in *cxcr4a*^{um20} mutants (Fig 1E and 1F). This suggests that the organ localization defects are not secondary effects of impaired endoderm migration. Therefore, the *cxcr4a* expression in DFC/KV cells is required for L-R laterality. In addition, the deficiency of *cxcl12b* in *cxcl12b*^{mu100} mutants [37], was also found to result in laterality defects (Fig 1G and 1H), indicating that the Cxcl12b-Cxcr4a signaling pathway is critical for L-R symmetry breaking.

Because organ laterality is regulated by evolutionally conserved asymmetric L-R gene expression in vertebrates, we next examined the expression patterns of *spaw* and its downstream gene *pitx2c* [1,38]. At the late somite stages, we observed *spaw* and *pitx2c* expression in the left LPM in wild-type embryos, whereas expression of these genes was found to be bilateral or absent in *cxcr4a*^{um20} mutants and DFC$^{4a\ MO}$ embryos (Fig 1I-1N). Interestingly, the bilateral expression domain of *spaw* in a subset of *cxcr4a*^{um20} mutants was located in the more posterior region in the LPM (Fig 1I), indicating a delay in the anterior spreading of *spaw* expression.

Collectively, these results demonstrate a sustaining expression of *cxcr4a* in the DFC/KV cells and implicate a crucial role of Cxcl12b-Cxcr4a chemokine signaling in L-R laterality determination.

Ablation of *cxcr4a* compromises KV organogenesis and ciliogenesis

To determine whether a loss of *cxcr4a* alters KV morphogenesis, we first

examined the formation of DFC clusters during gastrulation in *cxcr4a*^{um20} mutants carrying the transgenic DFC/KV reporter *sox17:GFP*. We observed that, in both wild-type embryos and *cxcr4a*^{um20} mutants, the GFP-positive DFCs were maintained as a cohesive group and migrated towards the vegetal pole during mid- to late-gastrulation (S2A Fig). Meanwhile, in comparison to control embryos, *cxcr4a*^{um20} mutants exhibited a normal expression pattern of *sox17* transcripts in the DFC clusters (S2B Fig). Based on these observations, we concluded that *cxcr4a* is unnecessary for the specification, clustering, and collective migration of DFCs.

We then examined the morphology of KV in live embryos at the 10-somite stage, at which point KV was well formed [4]. Wild-type embryos exhibited a normal button-like KV at the terminus of the notochord, as observed under bright-field microscopy (Fig 2A). In contrast, a large majority of *cxcr4a*^{um20} mutants displayed a smaller or tiny/absent KV (Fig 2A and 2B). In order to monitor the dynamic changes during KV formation, we carried out *in vivo* time-lapse image analysis on *cxcr4a*-deficient *Tg(sox17:GFP)* embryos from the 1- to 6-somite stages. DFCs were found to have already rearranged into a single rosette concurrent with the formation of the preliminary lumen in 1-somite stage wild-type and *cxcr4a*^{um20} mutant embryos (Fig 2C). However, the GFP-positive KV appeared to be dramatically smaller in *cxcr4a*^{um20} embryos in comparison to control animals from the 3- to 6-somite stages (Fig 2C). We next looked into the apical-basal polarity of KV epithelial cells, which is critical for the correct establishment of L-R asymmetry [39]. Immunostaining experiments revealed that the distributions of the basal-lateral marker E-cadherin and

the apical marker aPKC in KV epithelial cells of 10-somite stage *cxcr4a*^{um20} embryos were correct (S2C-S2D Fig). These observations suggest that *cxcr4a* is critical for organ size control, but is not required for epithelial cell polarization during KV organogenesis.

Monocilia in KV are known to generate a counter-clockwise fluid flow, which creates asymmetrical signals required to break L-R symmetry [4]. We next analyzed KV cilia formation by probing for acetylated tubulin (α-Tubulin) in the *cxcr4a*^{um20} embryos at the 10-somite stage. We found that, in comparison with control embryos, *cxcr4a*^{um20} mutants exhibited a significant decrease in cilia number and a steady reduction in cilia length (Fig 2D-2F). We then sought to determine whether the KV directional fluid flow was altered in *cxcr4a*^{um20} mutants. Fluorescent beads were injected into KVs at the 6-somite stage and the movements of the beads were tracked at the 10-somite stage. The fluorescent beads moved in a persistent counter-clockwise fashion in wild-type embryos, whereas they exhibited no directional flow in *cxcr4a*-deficient embryos (Fig 2G; S1-S2 Videos). Therefore, these results indicated that *cxcr4a* is indispensable for KV ciliogenesis and cilia-driven fluid flow.

Absence of *cxcr4a* attenuates G1/S transition and zFoxj1a protein expression

Our studies suggest that *cxcr4a* deficiency leads to smaller KV size as well as fewer KV cilia. Interestingly, the majority of the KV epithelial cells in *cxcr4a* mutants exhibited an intact apical-basal polarity and formed notably shortened cilia (Fig 2D and S3C-S3D Fig). This suggests that the altered KV cilia numbers may be caused by

defects in cell proliferation. To address this issue, we first examined the proliferation profile of DFC/KV cells by performing bromodeoxyuridine (BrdU) incorporation assays in *Tg(sox17:GFP)* embryos during gastrulation and early somite stages. Consistent with previous reports [16], approximately 70% of DFCs were positively stained with BrdU at the mid-gastrulation stage, whereas very few BrdU-positive cells were observed in the developing KV at the bud and the 6-somite stages (Fig 3A and 3B), suggesting that vigorous proliferation occurs in DFCs during epiboly stages and then declines at the end of gastrulation. Impressively, we found a dramatic decrease of the BrdU-positive DFC number in *cxcr4a*-deficient embryos at mid-gastrulation stage (Fig 3C and 3D), indicating a crucial requirement of *cxcr4a* in DFC proliferation.

We next examined the detailed effects of *cxcr4a* deficiency on DFC cycle progression in *Tg(sox17:GFP;EF1α:mKO2-zCdt1(1/190))* double transgenic embryos, a model in which cells in G1 phase exhibit red nuclear fluorescence [40]. Because the G1/S transition is very short in cells which undergo rapid mitotic cycles [40], we were unable to identify any mKO2-zCdt1-positive DFCs in both control embryos and *cxcr4a*^{um20} mutants during gastrulation. Interestingly, while the majority of cells in the developing KV enter into a quiescent state at the end of gastrulation (Fig 3A and 3B), we observed no or only few KV progenitors with mKO2-zCdt1 fluorescence (Fig 3E-3H). These results, combined with the previous observation that the mKO2-zCdt1 signal was highlighted in differentiated cells, including postmitotic neurons and muscle cells after the 10-somite stage [40], imply that there exist limitations in the ability to dissect cell-cycle behavior using this fluorescent indicator in early zebrafish

265 embryos. However, *cxcr4a* depletion resulted in a marked proportion of KV
266 progenitors with robust mKO2-zCdt1 expression, indicating impaired G1/S transition
267 and an apparent lengthening of the G1 phase (Fig 3E-3H). Nevertheless, our results
268 suggest that Cxcr4a-mediated chemokine signaling is responsible for driving DFC
269 proliferation by accelerating the G1/S transition. This provides an explanation for the
270 smaller KV size which was observed in *cxcr4a*^{um20} mutants.

271 Because zebrafish Foxj1a (zFoxj1a) is a master regulator of KV ciliogenesis
272 [19,20], we then sought to determine whether zFoxj1a expression was affected in
273 *cxcr4a*^{um20} mutants. *In situ* hybridization analysis demonstrated normal expression
274 levels of *zfoxj1a* transcripts in *cxcr4a*^{um20} embryos during gastrulation (S3 Fig). In
275 contrast, expression levels of zFoxj1a proteins were clearly decreased in *cxcr4a*^{um20}
276 mutants as revealed by immunostaining and western blot experiments (Fig 3I and 3J).
277 These analyses provide strong evidence that Cxcr4a signaling is responsible for
278 controlling KV ciliogenesis through regulation of zFoxj1a protein expression at the
279 post-transcription level.

280

281 **Cxcr4a-ERK1/2 cascade controls DFC proliferation by regulating cyclin D1**
282 **expression**

283 The Cxcl12-Cxcr4 axis is known to regulate cell-cycle progression through
284 GSK-3β/β-catenin and ERK1/2 signaling pathways [41-43]. To determine which of
285 these candidate pathways mediates Cxcr4-regulated DFC proliferation, *cxcr4a*^{um20}
286 mutant embryos were immunostained with antibodies against β-catenin or

phosphorylated ERK1/2 (p-ERK1/2) at the 75%-epiboly stage. No obvious changes in the cellular distribution of endogenous β-catenin in DFCs were observed in *cxcr4a*^{um20} mutants (S4 Fig), indicating that GSK-3β/β-catenin signaling is not altered with *cxcr4a* depletion. However, we found a robust expression of p-ERK1/2 in wild-type DFCs, which was nearly abolished in *cxcr4a*-deficient cells (Fig 4A). Strikingly, DFC-specific overexpression of MEK1$^{S219D, S223D}$, a constitutively activated version of MEK1 (caMEK1) [44], rescued the L-R defects in *cxcr4a*^{um20} mutants in a dose-dependent manner (Fig 4B-4E). Therefore, these results demonstrate a role for ERK1/2 signaling downstream of Cxcr4 in organ laterality.

Among the cell-cycle-regulatory genes, Cyclin D1 expression is known to be specifically activated by the Cxcr4a-ERK1/2 cascade to promote cell proliferation [41,42,45]. Consistent with these previous studies, double fluorescence *in situ* hybridization analyses indicated a dramatic reduction in *cyclin D1* expression in *cxcr4a*-deficient DFCs (Fig 4F). In addition, the introduction of caMEK mRNA counteracted the *cxcr4a* depletion effects on *cyclin D1* expression (Fig 4F). Cell cycle progression from G1 to the S phase is governed by CDK4/6 and CDK2, which are activated by D-type and E- or A-type cyclins, respectively [7]. Interestingly, upon exposure of wild-type embryos to PD0332991, a selective CDK4/6 inhibitor [46], from the shield stage to the bud stage, the resulting animals exhibited L-R defects similar to those observed in *cxcr4a*^{um20} mutants (Fig 4G and 4H). At the same time, embryos treated with CYC202, a selective CDK2 inhibitor [47], showed no significant changes in laterality development (Fig 4G and 4H). These results suggest

309 that Cyclin D1-CDK4/6 complexes play critical roles in DFC proliferation and L-R
310 asymmetric development. Importantly, reintroduction of *cyclin D1* into DFCs was
311 found to relieve the inhibition of cell proliferation, the reduction of KV size, and the
312 defects of organ laterality in *cxcr4a*^{um20} mutants (Fig 4I-4M). Collectively, our data
313 indicate that the Cxcr4a-ERK1/2 cascade functions in DFC proliferation through
314 regulation of Cyclin D1 expression during zebrafish L-R development.
315

316 **CDK4 and its kinase activity is required for Foxj1 protein stabilization**

317 Because the injection of *cyclin D1* mRNA into DFCs was found to rescue the L-R
318 defects in *cxcr4a*^{um20} mutants (Fig 4L and 4M), we hypothesized that Cyclin D1 acts
319 downstream of Cxcr4a signaling to control both cell proliferation and cilia formation.
320 In support of this hypothesis, upon injection of 300 pg *cyclin D1* mRNA into
321 mid-blastula stage *cxcr4a*^{um20} embryos, we observed that both the number and the
322 length of KV cilia were restored (Fig 5A-5C), indicating a role of Cyclin D1 in
323 ciliogenesis. It is surprising that the DFC-specific delivery of *cyclin D1* mRNA was
324 also able to restore the expression of endogenous Foxj1a protein in *cxcr4a*^{um20}
325 embryos (Fig 5D).

326 We next aimed to understand whether Foxj1 protein stability is regulated by
327 Cyclin D1-CDK4/6 complexes. As depicted in Fig 5E, Cyclin D1 or CDK4
328 overexpression in HEK293T cells notably increased zFoxj1a expression. This
329 increase in exogenously expressed zFoxj1a was even more apparent when Cyclin
330 D1-CDK4 complexes were ectopically expressed (Fig 5E). We noted that Cyclin

D1-CDK4 complexes also showed similar effects on the expression levels of mouse Foxj1 (mFoxj1) (Fig 5F). In combination with our observation of unchanged *foxj1a* transcript expression in *cxcr4a*^{um20} mutants, these results suggest that Cyclin D1-CDK4 complexes may play crucial roles in the prevention of Foxj1a protein degradation. Indeed, we observed that the treatment of MG132, a proteasome inhibitor, but not NH4Cl, a lysosome inhibitor, or 3-methyladenine (3-MA), a well-characterized inhibitor of autophagy, dramatically stabilized zFoxj1a protein (Fig 5G). In contrast, blocking endogenous CDK activity with PD0332991 treatment was found to result in a clear reduction of zFoxj1a expression (Fig 5H). In addition, the PD0332991 treatment-induced zFoxj1a turnover was completely suppressed by co-treatment with MG132 (Fig 5H). Therefore, Cyclin D1-CDK4 complexes contribute to Foxj1 protein stabilization. To further determine whether CDK4 kinase activity is important for Foxj1 protein stability, we generated a zebrafish kinase deficient mutant denoted CDK4-K38M, in which the ATP-binding site (Lys-38) in the catalytic subunit was mutated to a methionine residue [48]. As shown in Fig 5I, ectopic expression of CDK4-K38M had no effect on the zFoxj1a expression and PD0332991 treatment eliminated CDK4-mediated protein stabilization. These data suggest that CDK4 stabilizes Foxj1 through its kinase activity.

CDK4 physically interacts with and directly phosphorylates Foxj1

To understand whether Foxj1 is a substrate of CDK4 kinase, we first examined the possible interaction between these two proteins. HeLa cells were transiently

353 transfected with Flag-tagged zFoxj1a and Myc-tagged CDK4. Immunofluorescence
354 staining experiments revealed a colocalization of overexpressed zFoxj1a and CDK4 in
355 the nuclear aggregates (Fig 6A), suggesting a potential interaction between these two
356 proteins. As zFox1a was observed to be localized exclusively to the nucleus, even
357 when co-expressed with CDK4 (Fig 6A), we excluded the effects of CDK4 on the
358 subcellular distribution of zFox1a. We next examined the association between zFoxj1
359 and CDK4 in wild-type embryos and HEK293T cells. Co-immunoprecipitation
360 experiments demonstrated that overexpressed CDK4 interacted with endogenous and
361 ectopically expressed zFoxj1a (Fig 6B and 6C). Interestingly, the kinase deficient
362 form of CDK4 failed to associate with zFoxj1a (Fig 6C). In order to test whether
363 CDK4 interacts directly with Foxj1 protein, we carried out an *in vitro* binding assay
364 using purified proteins. As depicted in Fig 6D, Myc-CDK4 protein purified from
365 bacterial cells was able to bind to GST-zFoxj1a but not GST proteins. Collectively,
366 these results demonstrate that CDK4 interacts directly with zFoxj1a protein.

367 It is well established that the CDK families of serine/threonine protein kinases
368 phosphorylate substrates containing the consensus amino acid sequence (S/T)PXR/K
369 [49]. Because Cyclin D1-CDK4 complexes contribute to the stabilization of both
370 mouse and zebrafish Foxj1 (Fig 5E and 5F), we hypothesized that CDK4 is involved
371 in the phosphorylation of Foxj1 within conserved classic substrate motifs.
372 Interestingly, we found that zFoxj1a contains a potential CDK phosphorylation motif
373 “TPGK” at the N-terminal region, which is highly conserved in vertebrates (Fig 6E).
374 To investigate whether CDK4 phosphorylates Foxj1 protein, a

phospho-threonine-proline antibody was used to enrich CDK substrates from whole cell lysates, and the presence of phosphorylated Foxj1 was examined by western blot. With these experiments, we found that CDK4 or Cyclin D1-CDK4 complexes could effectively phosphorylate zFoxj1a and mFoxj1 (Fig 6F and S5A). As expected, CDK4-K38M almost lost the ability to induce zFoxj1a phosphorylation (Fig 6F). These results clearly indicate that Foxj1 can be phosphorylated by CDK4.

We then aimed to determine whether the threonine 102 residue (T102) within the putative conserved substrate motif of zFoxj1a is a major CDK phosphorylation site. Excitingly, we observed that Cyclin D1-CDK4 complexes significantly promoted wild-type zFoxj1a phosphorylation, which was nearly abolished in T102 mutant, an unphosphorylated form of zFoxj1a (Fig 6G). Similarly, *in vitro* phosphorylation assays showed that purified CDK4 or Cyclin D1-CDK4 complexes resulted in distinct phosphorylation events when incubated with recombinant wild-type zFoxj1a protein, but not T102 mutant (Fig 6H). In addition, we observed an increased expression of wild-type zFoxj1a while not its T102 mutant in HEK293T cells upon co-expression with CDK4 (Fig 6I). Similarly, CDK4 was able to control mFoxj1 stabilization through phosphorylation of the T87 residue, located in the conserved substrate motif (S5B-S5C Fig). Taken together, we showed that CDK4 directly phosphorylates Foxj1 to suppress its degradation.

zFoxj1a undergoes Ubiquitin-independent proteasomal degradation via a direct interaction with Psmd4b

Previous studies have suggested a primary role of the ubiquitin-proteasome system in the elimination of abnormal proteins and selective destruction of regulatory proteins [50,51]. To explore whether ubiquitination is required for Foxj1 degradation, we examined the effect of Ub K48R/G76A overexpression on zFoxj1a degradation. If zFoxj1a degradation was determined to be ubiquitylation-dependent, we would expect zFoxj1a to be stabilized upon overexpression of Ub K48R/G76A, which serves as a dominant negative inhibitor of poly-Ub chain formation [52,53]. Indeed, the presence of Ub K48R/G76A but not wild-type Ub efficiently inhibited the turnover of β-catenin (S6A Fig), which would be phosphorylated by glycogen synthase kinase-3β and destined for ubiquitin-mediated degradation [54]. Unexpectedly, overexpression of Ub K48R/G76A was unable to promote the stabilization of Flag-tagged zFoxj1a (S6A Fig). Because the Flag epitope contains two lysine residues, we generated a lysine-free version of zFoxj1a, termed HA-zFoxj1a-K20R by replacing the Flag tag with the HA epitope and mutating all 20 lysine residues within zFoxj1a protein to arginine residues. We found that both the wild-type and lysine-less zFoxj1a were significantly stabilized with CDK4 overexpression (S6B Fig). Therefore, zFoxj1a is able to be degraded independently of ubiquitylation.

Increasing evidence suggests that a list of proteins which directly interact with proteasomal subunits are thought to be degraded through an ubiquitin-independent degradation mechanism [55]. It has been demonstrated that the 19S regulatory subunit Rpn10 plays a critical role in the recognition of ubiquitin-independent substrates [56-58]. Therefore, we examined whether zFoxj1a binds to zebrafish Psmd4b, the

ortholog of mammalian Rpn10. Indeed, overexpressed or endogenous zFoxj1a was found to interact with Psmd4b (Fig 7A and 7B). Consistent with these observations, an *in vitro* binding assay revealed a direct binding between purified zFoxj1a and Psmd4b (Fig 7C).

To further unveil how CDK4 and its kinase activity regulate Foxj1 stabilization, we examined whether CDK4 functions to control the interaction between Psmd4b and zFoxj1a. As expected, ectopic expression of wild-type CDK4, but not its kinase deficient mutant, dramatically suppressed the association of Psmd4b with zFoxj1a or zFoxj1a-K20R (Fig 7D and 7E). In contrast, the binding ability of the unphosphorylated form of zFoxj1a for Psmd4b was retained with CDK4 co-expression (Fig 7F). Interestingly, the phospho-mimicking mutant of zFoxj1a (zFoxj1a-T102D) completely lost its ability to bind Psmd4b (Fig 7G), suggesting that CDK4-mediated phosphorylation of zFoxj1a at T102 eliminates its affinity for Psmd4b. In addition, Psmd4b overexpression reduced the expression levels of zFoxj1a and its lysine-free mutant (Fig 7H). When HEK293T cells were transfected with same amount of plasmid DNA to express wild-type zFoxj1a and its T102A and T102D mutants, respectively, we detected the highest expression level of zFoxj1a-T102D (Fig 7I). However, T102D mutant could not be further stabilized by CDK4 overexpression (Fig 7I). Taken together, these results indicate that CDK4 phosphorylates and stabilizes zFoxj1a by disrupting its association with Psmd4b.

We next addressed the developmental relevance of CDK4-induced zFoxj1a stabilization. *Cxcr4a-deficient* DFCs exhibited defective *cycling D1* expression and

441 impaired G1/S transition (Fig 3E-3H and 4F), implying a dysregulated activation of
442 the CDK4/6 kinases. DFC-specific overexpression of zFoxj1a-T102D, but not
443 wild-type or zFoxj1a-T102A, was found to restore the length of KV cilia in
444 *cxcr4a*^{um20} mutants (Fig 7J and 7K). As zFoxj1a is not involved in DFC proliferation
445 [19,20], it was reasonable to find that the decrease in the number of cilia was not
446 alleviated (S7 Fig). Overall, our results support a model in which Cxcl12b/Cxcr4a
447 signaling activates ERK1/2, which then promotes Cyclin D1 expression. This in turn
448 activates CDK4/6 kinase activity in DFCs. These activated G1 CDKs drive G1/S
449 transition during DFC proliferation and promote zFoxj1a stability by phosphorylation
450 to support KV ciliogenesis at later stages (Fig 7L).
451

452 **Discussion**

453 In zebrafish embryos, DFCs undergo mitotic proliferation during epiboly and then
454 exit the cell cycle, giving rise to epithelial cells that assemble cilia in the mature KV
455 organ [16]. Cell cycle defects in DFCs are often accompanied by an alteration in KV
456 cilia elongation, raising the issue of whether there exists a feasible link between the
457 cell cycle and cilia formation [16]. In this study, our experiments resolve this issue by
458 demonstrating that Cxcr4 signaling is required for DFC proliferation and KV
459 ciliogenesis by promoting Cyclin D1 expression. Specifically, we found that Cyclin
460 D1-CDK4/6 accelerates the G1/S transition in DFCs, while also facilitates cilia
461 formation via stabilization of zFoxj1a. Ciliary dynamics appear to be precisely
462 coordinated with cell cycle progression [59]. It has been suggested previously that cell

463 quiescence is essential for the formation of mouse nodal cilia [60]. Indeed, we
464 observed that proliferating DFCs enter into a quiescent state upon differentiation into
465 ciliated epithelial KV cells. Interestingly, our data indicates that during epiboly stages,
466 Cxcr4a signal-induced expression of Cyclin D1 functions to regulate DFC
467 proliferation and zFoxj1a stability, which is important for the ciliogenesis of quiescent
468 KV cells. Therefore, the rapid cell cycle progression of DFCs during epiboly stages is
469 not only required for the generation of enough cells to construct KV, but also plays a
470 critical role in reserving sufficient levels of zFoxj1a protein to support subsequent
471 cilia formation. Because Wnt/β-catenin signaling has been reported to play a role in
472 both DFC proliferation and KV cilia elongation [21,61], it is interesting to consider
473 whether this signaling pathway contributes to zFoxj1a stabilization via regulation of
474 cell cycle progression during the establishment of L-R asymmetry.

475 It has been reported previously that G1 cyclins function together with their
476 associated CDKs to phosphorylate a variety of transcription factors, including
477 Smad2/3 and pluripotency factors, to control embryonic stem (ES) cell differentiation
478 [11,12]. A systematic screen for CDK4/6 substrates identified fox family transcription
479 factor FOXM1 as a critical phosphorylation target [62]. CDK4/6 stabilize and activate
480 FOXM1 by phosphorylation at multiple sites to protect cancer cells from senescence
481 [62]. In contrast, CDK2 reduces DNA damage-induced cell death by phosphorylation
482 of FOXO1 at Ser249, resulting in cytoplasmic localization of FOXO1 [63]. In this
483 study, we show that CDK4 directly interacts with and phosphorylates zFoxj1a at a
484 conserved “TPGK” motif within the N-terminal region. Phosphorylation at T102 was

not found to alter the subcellular distribution of zFoxj1a, but was shown to promote its stabilization. Therefore, the functional interaction between CDK4 and zFoxj1a provides a mechanism by which cilia development is facilitated. Because CDK4 also stabilizes mFoxj1 through phosphorylation of T87 within the substrate motif, it is likely that the molecular linkage between cell-cycle progression and ciliogenesis is conserved among vertebrates.

The majority of proteosomal protein degradation relies on Ub conjugation. However, there are increasing numbers of examples of proteasomal degradation which occur without prior ubiquitination [64,65]. Our study reveals that overexpression of the dominant-negative Ub has no effect on zFoxj1a stabilization. However, wild-type and lysine-less zFoxj1a are found to be similarly stabilized by ectopic CDK4 expression. Therefore, zFoxj1a is targeted for proteasomal degradation in an Ub-independent manner. Intriguingly, E3 Ub ligases, including MGRN1 and Lnx2b, have been reported to play a role in L-R laterality specification in rodents and zebrafish [23,66], suggesting a role of the Ub-proteasome system in the modulation of protein turnover during L-R body patterning. However, due to the fact that L-R symmetry breaking occurs within a short time window during vertebrate embryonic development [4,67], the accelerated and economical regulation of protein degradation may be essential. Because Ub-independent degradation does not require the enzymatic cascade of Ub-conjugation, it would be more efficient to alter the concentration of zFoxj1a protein levels via Ub-independent proteasomal degradation during L-R asymmetric development. Interestingly, a recent study has demonstrated

that Foxj1 is rapidly turned over by the Ub-proteasome system in mouse primary ependymal cells [68]. Therefore, Foxj1 is a protein with a short half-life which undergoes proteasomal degradation via Ub-dependent or -independent pathways dependent on the cellular context.

Several proteins have been reported to interact with the 19S regulatory subunit Rpn10 via their Ub-like (UBL) domains [56-58]. Interestingly, while lacking a UBL-domain, zFoxj1a interacts directly with Psmd4b, the zebrafish ortholog of mammalian Rpn10. Our study demonstrates that CDK4 phosphorylates and stabilizes zFoxj1a by disrupting its association with Psmd4b. Similarly, the Ub-independent proteasomal degradation of Yeast Pah1 has also shown to be governed by its phosphorylation state [69]. Therefore, this may represent a general mechanism by which protein kinase-mediated phosphorylation plays a critical role in the protection of their substrates from Ub-independent proteasomal degradation.

Materials and methods

Zebrafish strains

Wild-type embryos were obtained from natural matings of Tuebingen zebrafish. Embryos were raised in Holtfreter's solution at 28.5 °C and staged by morphology. *cxcr4a* mutant embryos were generated by crossing homozygous male and female *cxcr4a*^{mu20} adult mutants. *Tg(sox17:GFP)* transgenic embryos were used to indicate the DFCs and KV cells during L-R asymmetric development. *Tg(EF1α:mKO2-zCdt1(1/190))* transgenic embryos express the fluorescent fusion

529 protein mKO2-zCdt1(1/190) in cells at the G1 phase during embryonic development.
530 *Tg(flk:EGFP)* transgenic embryos express EGFP in blood vessels. Our zebrafish
531 experiments were all approved and carried out in accordance with the Animal Care
532 Committee at the Institute of Zoology, Chinese Academy of Sciences (Permission
533 Number: IOZ-13048).
534
535 **RNA synthesis, morpholinos and microinjection**
536 Capped mRNAs for *cxcr4a*, *caMEK1*, *cyclin D1*, *zfoxj1a*, *zfoxj1a-T102A* and
537 *zfoxj1a-T102D* were *in vitro* synthesized from corresponding linearized plasmids
538 using the mMessage mMachine kit (Ambion). Digoxigenin-UTP-labeled antisense
539 RNA probes were in vitro transcribed using the MEGAscript Kit (Ambion) according
540 to the manufacturer's instructions. The standard control morpholino
541 (5'-CCTCTTACCTCAGTTACAATTTATA-3') and splicing MO targeting *cxcr4a*
542 (5'-AGACGATGTGTTCGTAATAAGCCAT-3') were purchased from Gene Tools
543 (Philomath, OR, USA) and used as previously described [30,70]. For DFC-specific
544 knockdown or overexpression experiments, indicated MOs or mRNAs were injected
545 into the yolk at the 256-cell stage as described previously [36].
546
547 **Whole-Mount in situ hybridization**
548 Whole-mount *in situ* hybridization was performed using the NBT-BCIP substrate
549 following standard procedures. For two-color fluorescence *in situ* hybridization,
550 Anti-digoxigenin-POD (11633716001, Roche) and anti-fluorescein-POD

(11426346910, Roche) were used as primary antibodies to detect digoxigenin-labeled sox17 probes and fluorescein-labeled *cyclin D1* probes, respectively. Fluorescence *in situ* hybridization was then carried out using the Perkin Elmer TAS fluorescein system (NEL701A001KT) according to the manufacturer's instructions.

Cell lines and transfection

HEK293T and Hela cell lines (American Tissue Culture Collection, ATCC, USA) were cultured in DMEM medium supplemented with 10% FBS in a 37°C humidified incubator in a 5% CO_2 environment. Cell transfections were carried out using Lipofectamine 2000 (11668019, Invitrogen) following the manufacturer's instructions.

Immunostaining and confocal microscope

Embryos were fixed in 4% paraformaldehyde overnight. Fixed embryos were then rinsed with PBST for a total of 4 times every 5 minutes. Embryos were then blocked at room temperature for 1 hour in 10% heat-inactivated goat serum and then stained with the following affinity-purified primary antibodies overnight at 4°C: anti-β-Catenin antibody (1:500; ab6302, Abcam), anti-Cdh1 (1:200; GTX125890, GeneTex), anti-pERK1/2 (1:1000; 9101, Cell Signaling), anti-acetylated-Tubulin antibody (1:400; T6793, Sigma), anti-BrdU (1：1000; ab6326, Abcam), anti-α-PKC (1:200, sc-216, Santa Cruz), anti-GFP (1:1000; A-11122, Invitrogen), anti-GFP (1:1000; A-11120, Invitrogen), anti-Foxj1 (1:200; ab220028, abcam). Samples were

573 then washed three times with PBST, followed by incubation with secondary
574 antibodies, including DyLight 488-conjugated Goat anti-rabbit IgG (1:200;
575 711-545-152, Jackson), DyLight 594-conjugated Goat anti-mouse IgG (1:200;
576 715-585-150, Jackson), DyLight 488-conjugated AffiniPure goat anti-mouse IgG
577 (1:200; 715-545-150, Jackson) and DyLight 594-conjugated AffiniPure goat
578 anti-rabbit IgG (1:200; 711-585-152, Jackson) for 1 hour at room temperature. In
579 some experiments, DAPI (1:10000, Sigma) was used to stain nuclei. The stained
580 embryos were then embedded with 2% low melting agarose and imaged using a
581 Nikon A1R+ confocal microscope with identical settings.
582
583 **Pharmacological treatment**
584 To block CDK activity, embryos were treated with 0.5 μM PD0332991 (A8318,
585 Palbociclib) or 0.2 μM CY202 (A1723, Palbociclib) from the shield stage to the bud
586 stage. For CDK4/6 inhibition in cultured cells, HEK293T cells were treated with 0.5
587 μM PD0332991 for 5 hours prior to harvest. In order to examine which pathway is
588 required for zFoxj1a degradation, HEK293T cells were transfected with plasmids
589 expressing Flag-zFoxj1a and treated with 20 mM NH_4Cl (A116363, Aladdin), 20 μM
590 MG132 (M7449, Sigma) and 5 mM 3-MA (M9281, Sigma), respectively, for 5 hours
591 prior to harvest.
592
593 **Fluorescent beads tracking**
594 Fluorescent red beads of 1 uM diameter (1:500, 18660-5, Polysciences) were injected

595 into the KV of embryos at the 6-somite stage. The resulting embryos were then
596 embedded in 2% low melting agarose at the 10-somite stage for confocal imaging.
597 Beads tracking videos and images were processed using Image Pro 6.0.
598
599 **Antibodies and immunoprecipitation assays**
600 For immunoblotting experiments, we used the following affinity-purified antibodies:
601 Anti-Flag (1:5000; F2555, Sigma), anti-Myc (1:3000; M047-3, MBL), anti-HA
602 (1:3000; CW0092A, CW), anti-β-Tubulin (1:5000, CW0098M, CWBIO), and
603 anti-Foxj1 (1:200; ab220028, Abcam).
604 For coimmunoprecipitation assays, embryos or HEK293T cells were harvested
605 and lysed with TNE lysis buffer (10mM Tris-HCl, pH 7.5, 150 mM NaCl, 2 mM
606 EDTA, and 0.5% Nonidet P-40) containing a protease inhibitor mixture. Lysates were
607 incubated with anti-Flag-agarose beads (A2220, Sigma) or protein A-Sepharose beads
608 (101041, Invitrogen) and anti-phospho-Threonine-Proline antibody (1:5000; 9391,
609 Cell Signaling) at 4°C for 4 hours. Beads were washed four times with TNE buffer.
610 Bound proteins were then separated by SDS-PAGE and visualized by western blots.
611
612 **In vitro GST Pull-Down**
613 GST fusion proteins were expressed in Escherichia coli. strain BL21 and purified
614 using Glutathione-Sepharose 4B beads (71024800-GE, GE Healthcare).
615 GST-Myc-CDK4, GST-HA-cyclinD1, and GST-Flag-psmd4b were treated with
616 Thrombin (1:1000; T4648, Sigma) to cleave their GST tags. For *in vitro* binding

assays, GST-Foxj1a proteins were immobilized by Glutathione-Sepharose 4B beads and incubated with the indicated purified proteins at 4°C for 3 hours. Following washing, the bound proteins were separated with SDS-PAGE and analyzed by western blots.

In vitro kinase assay

For i*n vitro* kinase assays, 1 μg GST-Foxj1a or GST-Foxj1a-T102A was incubated with 1 μg of the indicated purified proteins in 1×kinase buffer (25 mM Tris-Cl, pH7.5, 5 mM β-glycerophosphate, 0.1 mM Na_3VO_4, 10 mM $MgCl_2$, 2 mM dithiothreitol) with or without 50 μM ATP (P0756S, New England Biolabs) at 30°C for 30 min. The mixture was then separated on 10% SDS-PAGE and visualized by western blots or Coomassie Blue staining.

Statistical analysis

Cilia number and length were measured using ImageJ software. All results were expressed as the mean ± SD. Differences between control and treated groups were analyzed using the unpaired two-tailed Student's *t*-test. Results were considered statistically significant at $p < 0.05$.

Acknowledgements

We are grateful to Dr. Jingwei Xiong (Peking University, China) for the *Tg(EF1α:mKO2-zCdt1(1/190))* fish line and Dr. Linfei Luo (Southwest University,

639 China) for *cxcr4a*^{mu20} and *cxcl12b*^{mu100} fish lines.

640

641 **References**

642 1. Grimes DT, Burdine RD (2017) Left-Right Patterning: Breaking Symmetry to
643 Asymmetric Morphogenesis. Trends Genet 33: 616-628.
644 2. Essner JJ, Amack JD, Nyholm MK, Harris EB, Yost HJ (2005) Kupffer's vesicle is
645 a ciliated organ of asymmetry in the zebrafish embryo that initiates left-right
646 development of the brain, heart and gut. Development 132: 1247-1260.
647 3. Hirokawa N, Tanaka Y, Okada Y, Takeda S (2006) Nodal flow and the generation
648 of left-right asymmetry. Cell 125: 33-45.
649 4. Matsui T, Bessho Y (2012) Left-right asymmetry in zebrafish. Cell Mol Life Sci 69:
650 3069-3077.
651 5. Maclean K, Dunwoodie SL (2004) Breaking symmetry: a clinical overview of
652 left-right patterning. Clin Genet 65: 441-457.
653 6. Ramsdell AF (2005) Left-right asymmetry and congenital cardiac defects: getting
654 to the heart of the matter in vertebrate left-right axis determination. Dev Biol
655 288: 1-20.
656 7. Sherr CJ, Roberts JM (1999) CDK inhibitors: positive and negative regulators of
657 G1-phase progression. Genes Dev 13: 1501-1512.
658 8. Dalton S (2015) Linking the Cell Cycle to Cell Fate Decisions. Trends Cell Biol 25:
659 592-600.
660 9. Dalton S (2013) G1 compartmentalization and cell fate coordination. Cell 155:

13-14.

10. Julian LM, Carpenedo RL, Rothberg JL, Stanford WL (2016) Formula G1: Cell cycle in the driver's seat of stem cell fate determination. Bioessays 38: 325-332.

11. Pauklin S, Vallier L (2013) The cell-cycle state of stem cells determines cell fate propensity. Cell 155: 135-147.

12. Liu L, Michowski W, Inuzuka H, Shimizu K, Nihira NT, et al. (2017) G1 cyclins link proliferation, pluripotency and differentiation of embryonic stem cells. Nat Cell Biol 19: 177-188.

13. Lange C, Huttner WB, Calegari F (2009) Cdk4/cyclinD1 overexpression in neural stem cells shortens G1, delays neurogenesis, and promotes the generation and expansion of basal progenitors. Cell Stem Cell 5: 320-331.

14. Cooper MS, D'Amico LA (1996) A cluster of noninvoluting endocytic cells at the margin of the zebrafish blastoderm marks the site of embryonic shield formation. Dev Biol 180: 184-198.

15. Oteiza P, Koppen M, Concha ML, Heisenberg CP (2008) Origin and shaping of the laterality organ in zebrafish. Development 135: 2807-2813.

16. Gokey JJ, Dasgupta A, Amack JD (2015) The V-ATPase accessory protein Atp6ap1b mediates dorsal forerunner cell proliferation and left-right asymmetry in zebrafish. Dev Biol 407: 115-130.

17. Brody SL, Yan XH, Wuerffel MK, Song SK, Shapiro SD (2000) Ciliogenesis and left-right axis defects in forkhead factor HFH-4-null mice. Am J Respir Cell

683 Mol Biol 23: 45-51.

684 18. Chen J, Knowles HJ, Hebert JL, Hackett BP (1998) Mutation of the mouse
685 hepatocyte nuclear factor/forkhead homologue 4 gene results in an absence of
686 cilia and random left-right asymmetry. J Clin Invest 102: 1077-1082.

687 19. Yu X, Ng CP, Habacher H, Roy S (2008) Foxj1 transcription factors are master
688 regulators of the motile ciliogenic program. Nat Genet 40: 1445-1453.

689 20. Stubbs JL, Oishi I, Izpisua Belmonte JC, Kintner C (2008) The forkhead protein
690 Foxj1 specifies node-like cilia in Xenopus and zebrafish embryos. Nat Genet
691 40: 1454-1460.

692 21. Caron A, Xu X, Lin X (2012) Wnt/beta-catenin signaling directly regulates Foxj1
693 expression and ciliogenesis in zebrafish Kupffer's vesicle. Development 139:
694 514-524.

695 22. Neugebauer JM, Amack JD, Peterson AG, Bisgrove BW, Yost HJ (2009) FGF
696 signalling during embryo development regulates cilia length in diverse
697 epithelia. Nature 458: 651-654.

698 23. Kim MJ, Rhee M, Ro H (2014) Lnx2b, an E3 ubiquitin ligase, in dorsal forerunner
699 cells and Kupffer's vesicle is required for specification of zebrafish left-right
700 laterality. Animal Cells and Systems 18: 333-339.

701 24. Raz E, Mahabaleshwar H (2009) Chemokine signaling in embryonic cell
702 migration: a fisheye view. Development 136: 1223-1229.

703 25. Boldajipour B, Doitsidou M, Tarbashevich K, Laguri C, Yu SR, et al. (2011)
704 Cxcl12 evolution--subfunctionalization of a ligand through altered interaction

with the chemokine receptor. Development 138: 2909-2914.

26. Peled A, Petit I, Kollet O, Magid M, Ponomaryov T, et al. (1999) Dependence of human stem cell engraftment and repopulation of NOD/SCID mice on CXCR4. Science 283: 845-848.

27. Doitsidou M, Reichman-Fried M, Stebler J, Koprunner M, Dorries J, et al. (2002) Guidance of primordial germ cell migration by the chemokine SDF-1. Cell 111: 647-659.

28. David NB, Sapede D, Saint-Etienne L, Thisse C, Thisse B, et al. (2002) Molecular basis of cell migration in the fish lateral line: role of the chemokine receptor CXCR4 and of its ligand, SDF1. Proc Natl Acad Sci U S A 99: 16297-16302.

29. Knaut H, Werz C, Geisler R, Nusslein-Volhard C, Tubingen Screen C (2003) A zebrafish homologue of the chemokine receptor Cxcr4 is a germ-cell guidance receptor. Nature 421: 279-282.

30. Nair S, Schilling TF (2008) Chemokine signaling controls endodermal migration during zebrafish gastrulation. Science 322: 89-92.

31. Olesnicky Killian EC, Birkholz DA, Artinger KB (2009) A role for chemokine signaling in neural crest cell migration and craniofacial development. Dev Biol 333: 161-172.

32. Li L, Mao A, Wang P, Ning G, Cao Y, et al. (2018) Endodermal pouch-expressed dmrt2b is important for pharyngeal cartilage formation. Biol Open 7.

33. Siekmann AF, Standley C, Fogarty KE, Wolfe SA, Lawson ND (2009) Chemokine signaling guides regional patterning of the first embryonic artery.

727 Genes Dev 23: 2272-2277.

728 34. Chong SW, Emelyanov A, Gong Z, Korzh V (2001) Expression pattern of two
729 zebrafish genes, cxcr4a and cxcr4b. Mech Dev 109: 347-354.

730 35. Roussigne M, Bianco IH, Wilson SW, Blader P (2009) Nodal signalling imposes
731 left-right asymmetry upon neurogenesis in the habenular nuclei. Development
732 136: 1549-1557.

733 36. Amack JD, Yost HJ (2004) The T box transcription factor no tail in ciliated cells
734 controls zebrafish left-right asymmetry. Curr Biol 14: 685-690.

735 37. Bussmann J, Wolfe SA, Siekmann AF (2011) Arterial-venous network formation
736 during brain vascularization involves hemodynamic regulation of chemokine
737 signaling. Development 138: 1717-1726.

738 38. Hamada H, Meno C, Watanabe D, Saijoh Y (2002) Establishment of vertebrate
739 left-right asymmetry. Nat Rev Genet 3: 103-113.

740 39. Aw S, Levin M (2009) Is left-right asymmetry a form of planar cell polarity?
741 Development 136: 355-366.

742 40. Sugiyama M, Sakaue-Sawano A, Iimura T, Fukami K, Kitaguchi T, et al. (2009)
743 Illuminating cell-cycle progression in the developing zebrafish embryo. Proc
744 Natl Acad Sci U S A 106: 20812-20817.

745 41. Klein S, Abraham M, Bulvik B, Dery E, Weiss ID, et al. (2018) CXCR4 Promotes
746 Neuroblastoma Growth and Therapeutic Resistance through
747 miR-15a/16-1-Mediated ERK and BCL2/Cyclin D1 Pathways. Cancer Res 78:
748 1471-1483.

749 42. Mo W, Chen J, Patel A, Zhang L, Chau V, et al. (2013) CXCR4/CXCL12 mediate
750 autocrine cell- cycle progression in NF1-associated malignant peripheral nerve
751 sheath tumors. Cell 152: 1077-1090.
752 43. Wang Y, Xu P, Qiu L, Zhang M, Huang Y, et al. (2016) CXCR7 Participates in
753 CXCL12-mediated Cell Cycle and Proliferation Regulation in Mouse Neural
754 Progenitor Cells. Curr Mol Med 16: 738-746.
755 44. Bolcome RE, 3rd, Chan J (2010) Constitutive MEK1 activation rescues anthrax
756 lethal toxin-induced vascular effects in vivo. Infect Immun 78: 5043-5053.
757 45. Sherr CJ (1995) D-type cyclins. Trends Biochem Sci 20: 187-190.
758 46. Fry DW, Harvey PJ, Keller PR, Elliott WL, Meade M, et al. (2004) Specific
759 inhibition of cyclin-dependent kinase 4/6 by PD 0332991 and associated
760 antitumor activity in human tumor xenografts. Mol Cancer Ther 3: 1427-1438.
761 47. De Azevedo WF, Leclerc S, Meijer L, Havlicek L, Strnad M, et al. (1997)
762 Inhibition of cyclin-dependent kinases by purine analogues: crystal structure
763 of human cdk2 complexed with roscovitine. Eur J Biochem 243: 518-526.
764 48. Matsushime H, Ewen ME, Strom DK, Kato JY, Hanks SK, et al. (1992)
765 Identification and properties of an atypical catalytic subunit (p34PSK-J3/cdk4)
766 for mammalian D type G1 cyclins. Cell 71: 323-334.
767 49. Songyang Z, Blechner S, Hoagland N, Hoekstra MF, Piwnica-Worms H, et al.
768 (1994) Use of an oriented peptide library to determine the optimal substrates
769 of protein kinases. Curr Biol 4: 973-982.
770 50. Ciechanover A, Stanhill A (2014) The complexity of recognition of ubiquitinated

771 substrates by the 26S proteasome. Biochim Biophys Acta 1843: 86-96.

772 51. Johnson BM, DeBose-Boyd RA (2018) Underlying mechanisms for
773 sterol-induced ubiquitination and ER-associated degradation of HMG CoA
774 reductase. Semin Cell Dev Biol 81: 121-128.

775 52. Finley D, Sadis S, Monia BP, Boucher P, Ecker DJ, et al. (1994) Inhibition of
776 proteolysis and cell cycle progression in a multiubiquitination-deficient yeast
777 mutant. Mol Cell Biol 14: 5501-5509.

778 53. Ju D, Xie Y (2004) Proteasomal degradation of RPN4 via two distinct
779 mechanisms, ubiquitin-dependent and -independent. J Biol Chem 279:
780 23851-23854.

781 54. Liu C, Li Y, Semenov M, Han C, Baeg GH, et al. (2002) Control of beta-catenin
782 phosphorylation/degradation by a dual-kinase mechanism. Cell 108: 837-847.

783 55. Sanchez-Lanzas R, Castano JG (2014) Proteins directly interacting with
784 mammalian 20S proteasomal subunits and ubiquitin-independent proteasomal
785 degradation. Biomolecules 4: 1140-1154.

786 56. Hiyama H, Yokoi M, Masutani C, Sugasawa K, Maekawa T, et al. (1999)
787 Interaction of hHR23 with S5a. The ubiquitin-like domain of hHR23 mediates
788 interaction with S5a subunit of 26 S proteasome. J Biol Chem 274:
789 28019-28025.

790 57. Sakata E, Yamaguchi Y, Kurimoto E, Kikuchi J, Yokoyama S, et al. (2003)
791 Parkin binds the Rpn10 subunit of 26S proteasomes through its ubiquitin-like
792 domain. EMBO Rep 4: 301-306.

793 58. Du J, Zhang J, He T, Li Y, Su Y, et al. (2016) Stuxnet Facilitates the Degradation
794 of Polycomb Protein during Development. Dev Cell 37: 507-519.
795 59. Ford MJ, Yeyati PL, Mali GR, Keighren MA, Waddell SH, et al. (2018) A
796 Cell/Cilia Cycle Biosensor for Single-Cell Kinetics Reveals Persistence of
797 Cilia after G1/S Transition Is a General Property in Cells and Mice. Dev Cell
798 47: 509-523 e505.
799 60. Komatsu Y, Kaartinen V, Mishina Y (2011) Cell cycle arrest in node cells
800 governs ciliogenesis at the node to break left-right symmetry. Development
801 138: 3915-3920.
802 61. Zhang M, Zhang J, Lin SC, Meng A (2012) beta-Catenin 1 and beta-catenin 2
803 play similar and distinct roles in left-right asymmetric development of
804 zebrafish embryos. Development 139: 2009-2019.
805 62. Anders L, Ke N, Hydbring P, Choi YJ, Widlund HR, et al. (2011) A systematic
806 screen for CDK4/6 substrates links FOXM1 phosphorylation to senescence
807 suppression in cancer cells. Cancer Cell 20: 620-634.
808 63. Huang H, Regan KM, Lou Z, Chen J, Tindall DJ (2006) CDK2-dependent
809 phosphorylation of FOXO1 as an apoptotic response to DNA damage. Science
810 314: 294-297.
811 64. Erales J, Coffino P (2014) Ubiquitin-independent proteasomal degradation.
812 Biochim Biophys Acta 1843: 216-221.
813 65. Hwang J, Winkler L, Kalejta RF (2011) Ubiquitin-independent proteasomal
814 degradation during oncogenic viral infections. Biochim Biophys Acta 1816:

147-157.

66. Cota CD, Bagher P, Pelc P, Smith CO, Bodner CR, et al. (2006) Mice with mutations in Mahogunin ring finger-1 (Mgrn1) exhibit abnormal patterning of the left-right axis. Dev Dyn 235: 3438-3447.

67. Yoshiba S, Hamada H (2014) Roles of cilia, fluid flow, and Ca2+ signaling in breaking of left-right symmetry. Trends Genet 30: 10-17.

68. Abdi K, Lai CH, Paez-Gonzalez P, Lay M, Pyun J, et al. (2018) Uncovering inherent cellular plasticity of multiciliated ependyma leading to ventricular wall transformation and hydrocephalus. Nat Commun 9: 1655.

69. Hsieh LS, Su WM, Han GS, Carman GM (2015) Phosphorylation regulates the ubiquitin-independent degradation of yeast Pah1 phosphatidate phosphatase by the 20S proteasome. J Biol Chem 290: 11467-11478.

70. Ning G, Liu X, Dai M, Meng A, Wang Q (2013) MicroRNA-92a upholds Bmp signaling by targeting noggin3 during pharyngeal cartilage formation. Dev Cell 24: 283-295.

Figures and Figure legends

Figure 1

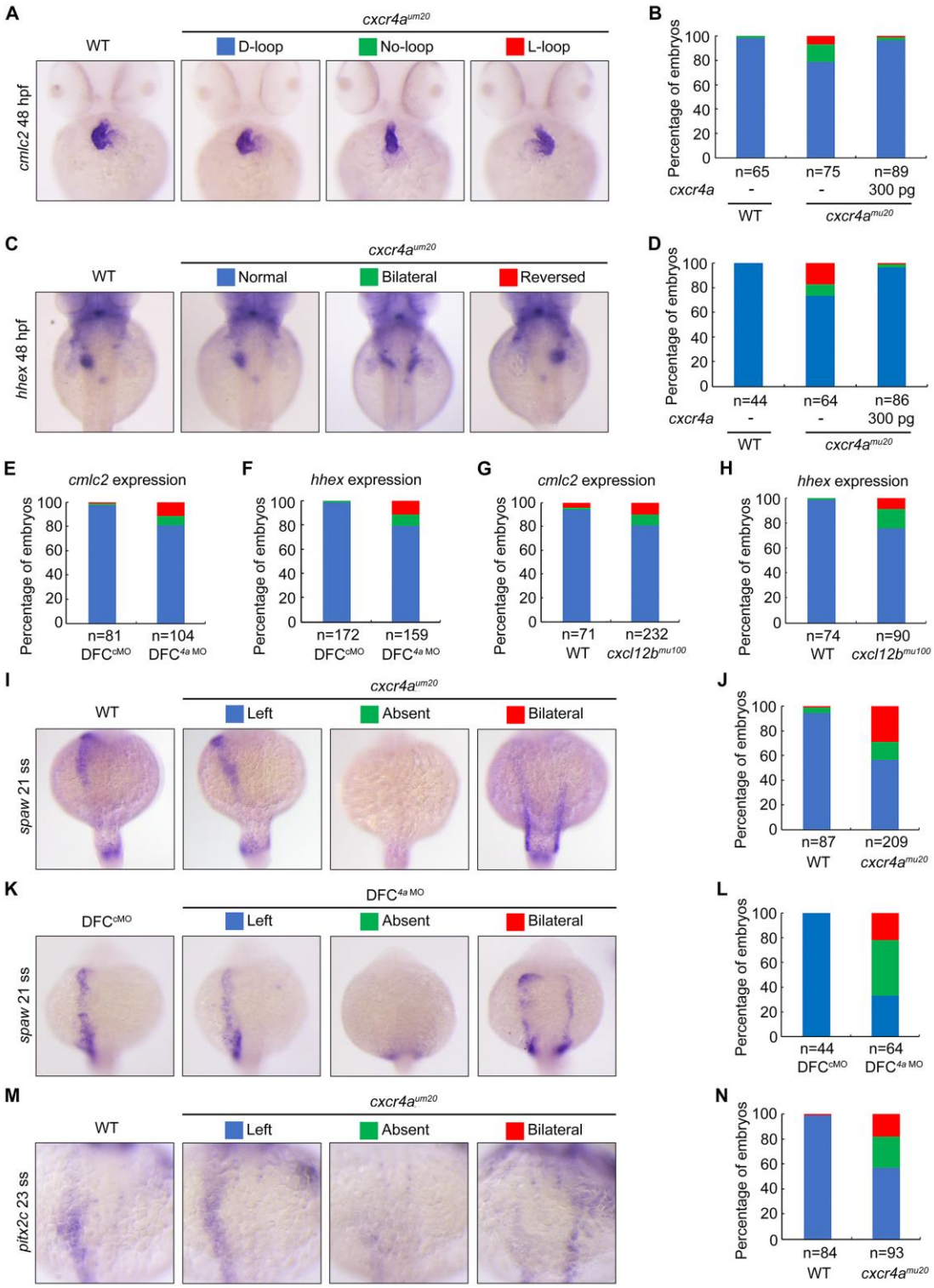

Fig 1. Cxcl12b-Cxcr4a signaling axis is essential for L-R asymmetric development. (A-D) Wild-type embryos and *cxcr4a*^{mu20} mutants injected with or without 300 pg *cxcr4a* mRNA at the 256-cell stage were examined for cardiac looping and liver laterality at 48 hpf by WISH against *cmlc2* (a) and *hhex* (C). Embryos with different phenotypes were shown in ventral (A) or dorsal view (C). Statistical data were shown in (B) and (D). (E-H) Statistical data for the expression patterns of *cmlc2* and *hhex* at 48hpf in wild-type embryos injected with 8 ng *cxcr4a* MO (4a MO) at the 256-cell stage (E and F) and *cxcl12b* mutants (G and H). (I-N) *cxcr4a* deficiency alters Nodal gene expression pattern. Representative images of *spaw* and *pitx2c* expression in *cxcr4a* mutants (I and M) and morphants (K). All embryos were shown in dorsal views with anterior on the top. Ratios of embryos were shown in (J, L and N).

Figure 2

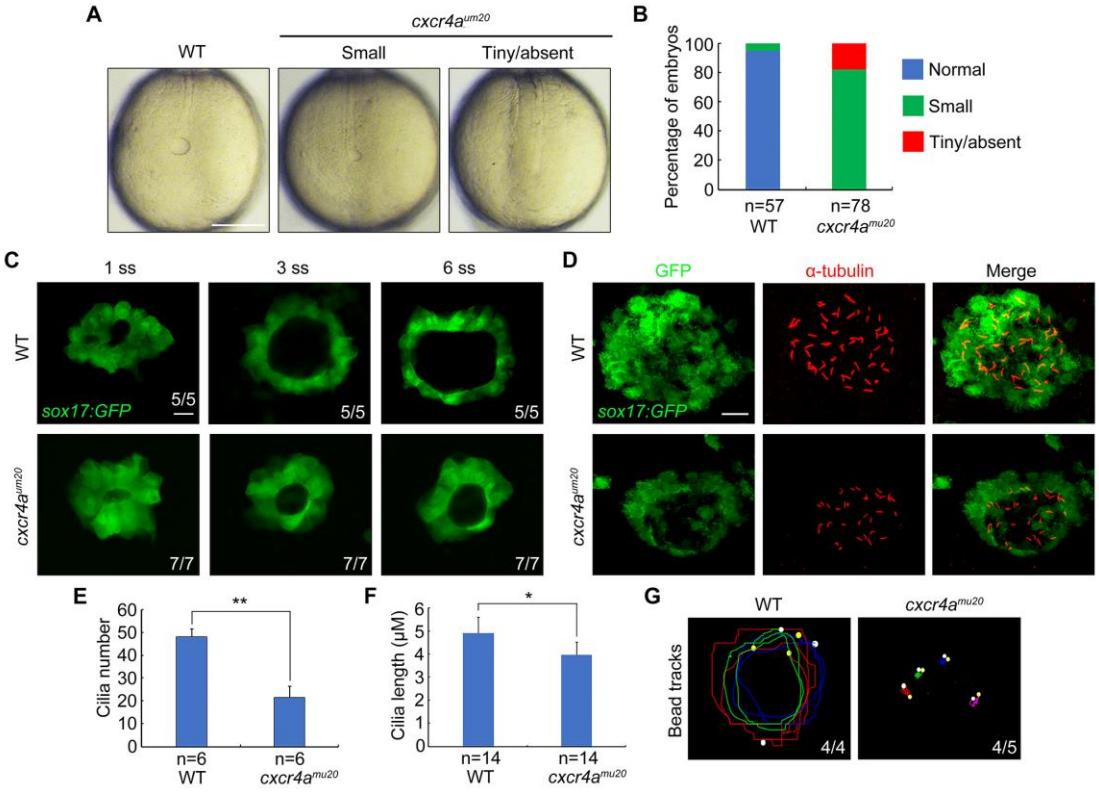

Fig 2. *cxcr4a* is indispensable for KV formation and ciliogenesis. (A-B) Light micrographs at the 10-somite stage showed smaller or even absent KVs in *cxcr4a*^{mu20} mutants. Scale bar, 200 μm. Embryo ratios with different KV sizes were shown in (B). (C) Time-lapse confocal images from the 1-somite stage to the 6-somite stage showed the dynamic formation of KV in wild-type and *cxcr4a* deficient *Tg(sox17:GFP)* embryos. Scale bar, 20 μm. The ratios of affected embryos was indicated. (D-F) Fluorescent immunostaining of KV using anti-GFP and anti-acetylated Tubulin antibodies at the 10-somite stage in wild-type embryos and *cxcr4a*^{mu20} mutants. Scale bar, 20 μm. Cilia average number and length were quantified from three independent experiments and the group values were expressed as the mean ± SD (E and F). Student's *t*-test, **P*<0.05, ***p* < 0.01. (G) Fluorescent bead tracking experiments showed that fluorescent beads moved in a persistent counter-clockwise fashion in wild-type embryos, but had no directional flow in *cxcr4a*^{mu20} mutants. White spots, yellow spots, and curves mark the start points, the end points, and the tracks of bead movements, respectively.

Figure 3

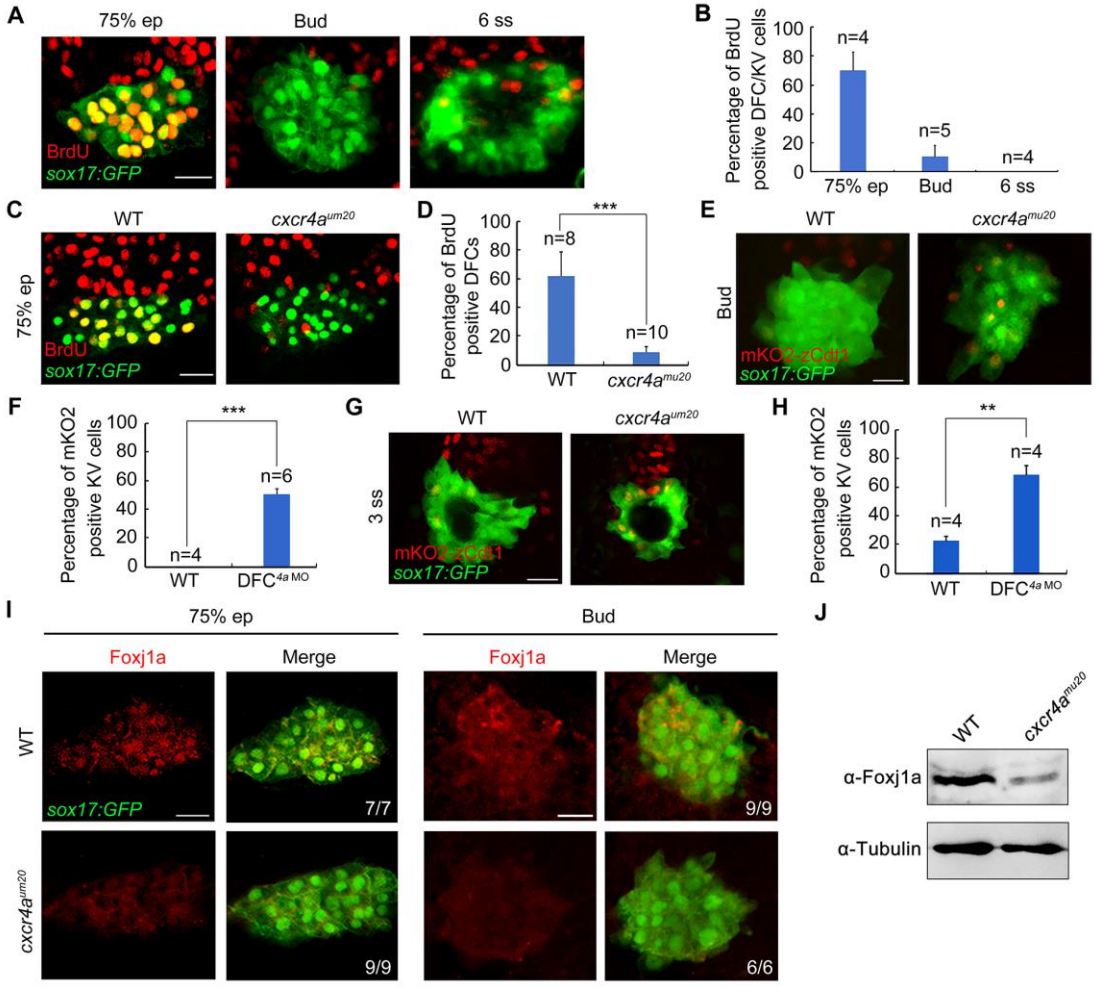

Fig 3. Depletion of *cxcr4a* impairs G1/S transition and Foxj1a protein expression in DFCs. (A-B) Representative confocal sections of BrdU-positive DFCs and KV cells at the indicated stages (A). Dorsal views with anterior on the top. Scale bar, 20 μm. The percentage of BrdU-positive cells among GFP-positive DFCs and KV cells were quantified from the indicated embryo numbers in three independent experiments and the group values are expressed as the mean ± SD (B). (C-D) BrdU incorporation experiments showed reduced proliferating DFCs in *cxcr4a*^{mu20} mutants at the 75% epiboly stage. Scale bar, 20 μm. Statistical data from three independent experiments was shown in (D). Student's *t*-test, ***P<0.001. (E-H) Depletion of *cxcr4a* inhibits the G1/S transition in DFCs. Representative confocal sections of wild-type and *cxcr4a*-deficient *Tg(sox17:GFP;EF1α:mKO2-zCdt1(1/190))* embryos at the bud and 3-somite stages were shown in (E and G). Dorsal views with anterior to the top. Scale bar, 20 μm. The percentage of mKO2-positive KV cells were quantified from three independent experiments (F and H). The significance of differences compared with the wild-type group were analyzed with the Student's *t*-test, **$p < 0.01$; ***$p < 0.001$. (I-J) *cxcr4a* deficiency downregulates zFoxj1a protein expression levels. Wild-type and *cxcr4a*-deficient *Tg(sox17:GFP)* embryos were harvested at the 75% epiboly and bud stages, and then subjected to immunostaining (I) and western blot analysis (J) with the indicated antibodies. Scale bar, 20 μm.

Figure 4

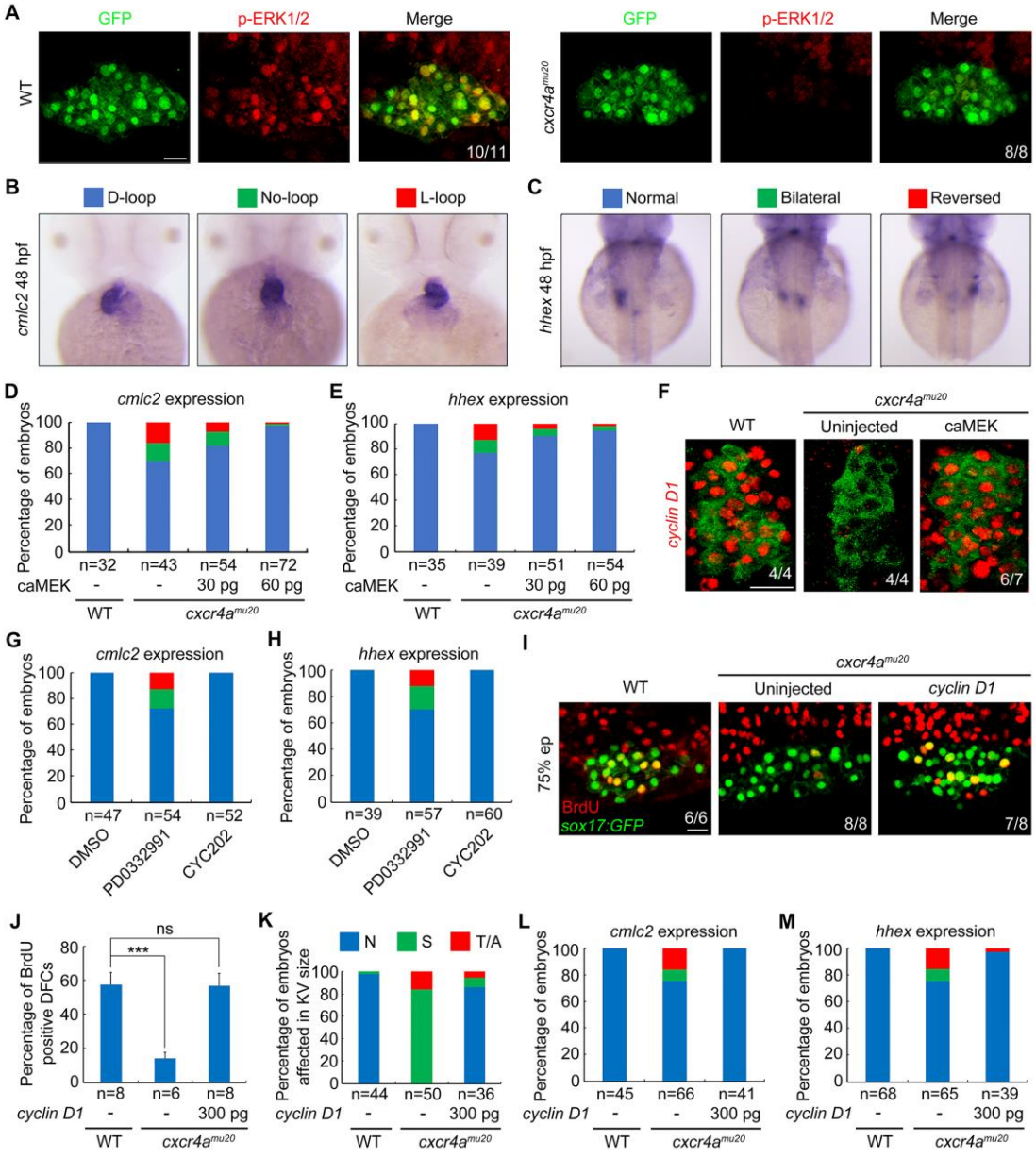

Fig 4. Cxcr4 promotes Cyclin D1 expression through ERK signaling during DFC proliferation. (A) ERK1/2 phosphorylation levels were dramatically decreased in *cxcr4a*^{mu20} mutants. Wild-type and *cxcr4a*-deficient *Tg(sox17:GFP)* embryos were harvested at the 75% epiboly stage and subjected to immunostaining for p-ERK1/2 (red) and GFP (green). All embryos were shown in dorsal views with anterior to the top. Scale bar, 20 μm. (B-E) caMEK mRNA overexpression in DFCs rescued L-R patterning defects in *cxcr4a*^{mu20} mutants. Different types of heart looping and liver laterality at 48 hpf in *cxcr4a*^{mu20} mutants following mid-blastula injection of different caMEK mRNA doses were visualized by *cmlc2* and *hhex* expression (B and C). Quantitative data were shown in (D and E). (F) *Cxcr4a*-deficient *Tg(sox17:GFP)* embryos were injected with 60 pg caMEK mRNA at the 256-cell stage, and then harvested at the 75% epiboly stage for fluorescence *in situ* hybridization experiments with *cyclin D1* (red) and GFP (green) probes. Dorsal views with anterior to the left. Scale bar, 20 μm. (G-H) Wild-type embryos were treated 0.5 μM PD0332991 or 0.2 μM CY202 from the shield stage to bud stage, and then analyzed for L-R patterning defects at 48 hpf by *in situ* hybridizations with *cmlc2* and *hhex* probes. The proportion of treated embryos exhibiting each type of heart looping and liver laterality were shown in (G) and (H). (I-J) Reintroduction of *cyclin D1* into DFCs relieves DFC proliferation defects in *cxcr4a*^{um20} mutants. *Cxcr4a*-deficient *Tg(sox17:GFP)* embryos were injected with or without 300 pg *cyclin D1* mRNA at the 256-cell stage, followed by coimmunostaining with anti-BrdU (red) and anti-GFP (green) antibodies at the 75% epiboly stage. Representative images were shown in (I) and the percentage of

BrdU-positive DFCs were indicated in (J). Scale bar, 20 μm. Student's *t*-test, ***$P<0.001$. ns, no significant difference.(K-M) Statistical data shows that DFC-specific overexpression of *cyclin D1* rescued the defects of KV formation (K) and L-R patterning (L and M) in *cxcr4a* mutants.

984 Figure 5

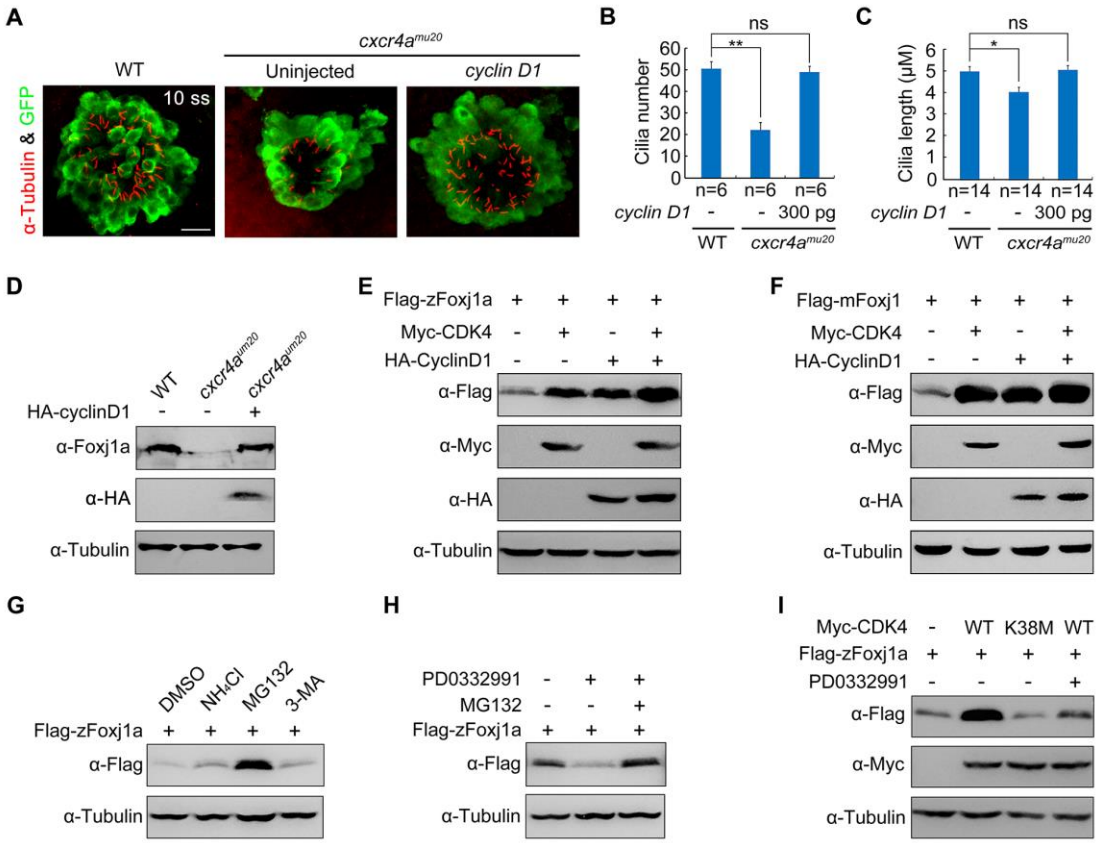

985

986

987

988

989

990

991

992

993

994

995

996

Fig 5. CDK4 stabilizes Foxj1 through its kinase activity. (A-C) Confocal images of 10-somite-stage *cxcr4a*-deficient *Tg(sox17:GFP)* embryos injected with or without 300 pg *cyclin D1* mRNA at the 256-cell stage (A). KV cells were labelled with antibodies against GFP (green) and cilia were visualized by acetylated tubulin immunofluorescence (red). Scale bar, 20 μm. Cilia number (B) and length (C) were analyzed. Student's *t*-test, **P*<0.05, ***P*<0.01. ns, no significant difference. Note that when *cyclin D1* mRNA was injected into *cxcr4a*-deficient DFCs, both the KV cilia number and length were restored. (D) Western blots of total lysates from 75% epiboly-stage wild-type embryos and *cxcr4a*^{um20} mutants injected with or without 300 pg *HA-cyclin D1* mRNA at the 256-cell stage. Tubulin was used as the loading control. Endogenous zFoxj1a protein levels in *cxcr4a*^{um20} mutants was rescued by DFC-specific overexpression of HA-cyclin D1. (E-F) CDK4 overexpression alone or together with Cyclin D1 results in an obvious increase in zFoxj1a (E) or mFoxj1 (F) expression. HEK293T cells were transfected with the indicated plasmids. Lysates were analyzed by western blot using the indicated antibodies. (G) HEK293T cells transfected with plasmids encoding Flag-zFoxj1a were treated with the lysozyme inhibitor NH4Cl (20 mM) or the proteasomal inhibitor MG132 (20 μM) or the autophagy inhibitor 3-MA (5 mM) for 5 hours prior to harvest for immunoblotting. (H) Lysates from Flag-zFoxj1a-expressing HEK293T cells treated with CDK4/6 inhibitor PD0332991 (0.5 μM) alone or in combination with MG132 (20 μM) were subjected to immunoblotting. (I) Overexpression of wild-type CDK4 but not its kinase mutant stabilizes zFoxj1a protein. HEK293T cells were transfected with the indicated

plasmids. PD0332991 (0.5 μM) was added 5 hours before harvest. Note that PD0332991 treatment blocked CDK4-induced zFOxj1a stabilization.

Figure 6

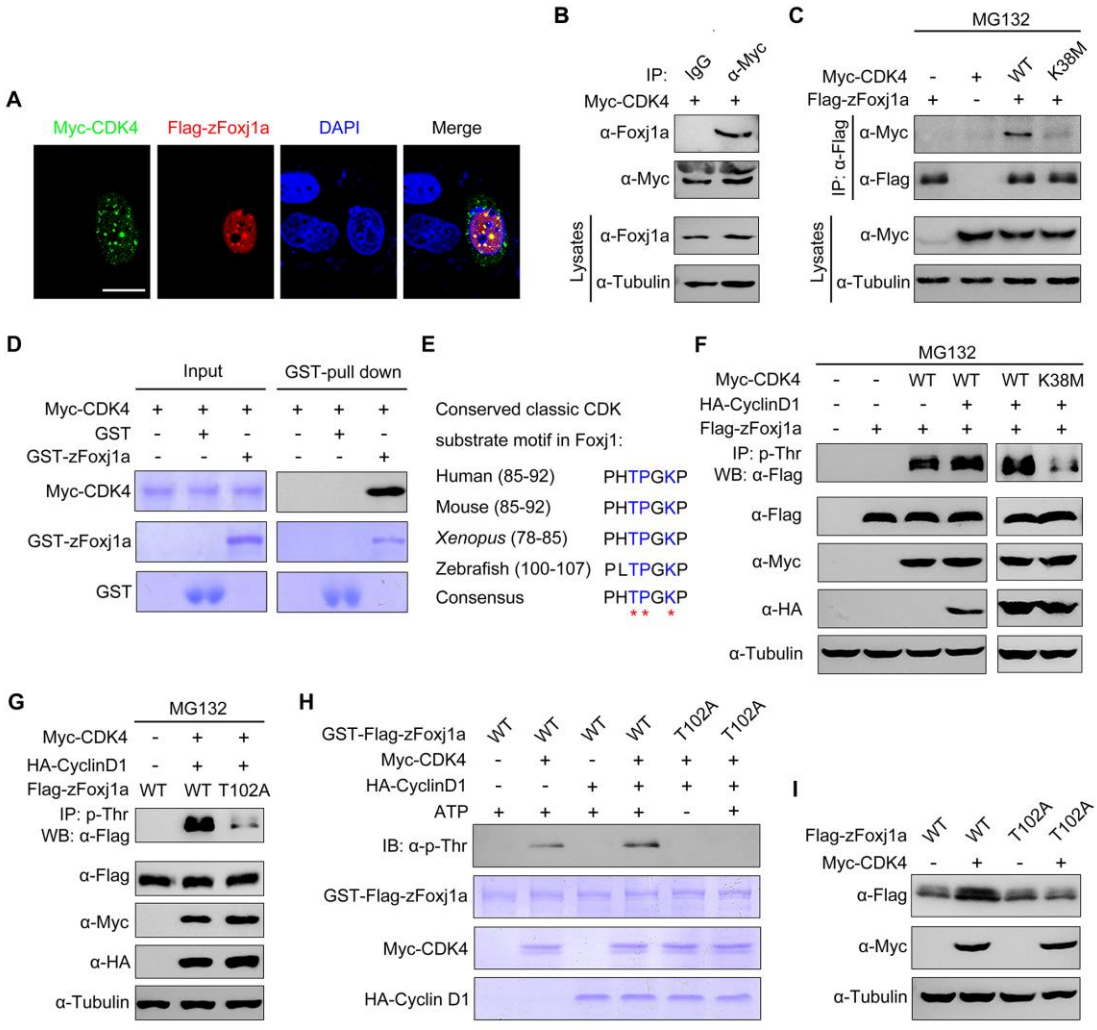

Fig 6. CDK4 phosphorylates zFoxj1a at T102 to suppress its degradation. (A) zFoxj1a and CDK4 show evident colocalization in Hela cells. Hela cells were transfected with Flag-zFoxj1a and Myc-CDK4 and immunostained with anti-Flag (red) and anti-Myc (green) antibodies. Nuclei were stained with DAPI (blue). Scale bar, 20 μm. (B) Overexpressed CDK4 interacts with endogenous zFoxj1a. Wild-type embryos were injected with 200 pg Myc-CDK4 mRNA at midgastrulation and then harvested at the bud stage for immunoprecipitation with anti-Myc antibody or normal mouse IgG. (C) CDK4 but not its kinase dead mutant interacts with zFoxj1a. HEK293T cells were transfected with plasmids as indicated, followed by treatment with MG132 for 5 hours prior to harvest for immunoprecipitation. (D) Direct binding of CDK4 to zFoxj1a *in vitro*. GST, GST- zFoxj1a and Myc-CDK4 were expressed in bacterial cells and purified. Myc-CDK4 proteins were incubated with GST or GST-zFoxj1a. The presence of Myc-CDK4 in the protein complex pull-downed by Glutathione agarose was assessed using an anti-Myc antibody. Input proteins were examined by Coomassie blue staining. (E) Conserved CDK substrate motifs in Foxj1 proteins from different species. Red stars indicate critical residues in the CDK substrate motifs.

(F-G) CDK4 phosphorylates zFoxj1a at T102. HEK293T cells were transfected with the indicated plasmids. CDK substrates were immunoprecipitated using a phospho-threonine-proline antibody and blotted with anti-Flag antibody to detect phosphorylated zFoxj1a or zFoxj1a-T102A. zFoxj1a-T102A is an unphosphorylated form of zFoxj1a. Note that wild-type zFoxj1a could be phosphorylated by CDK4 but not by the CDK4-K38M mutant (F). CDK4-mediated phosphorylation was nearly

abolished in zFoxj1a-T102A (G). (H) *In vitro* kinase assays revealed that CDK4 phosphorylates wild-type zFoxj1a but not the zFoxj1a-T102A mutant. zFoxj1a and zFoxj1a-T102A proteins were purified from bacterial cells and incubated with recombinant Cyclin D1 and CDK4 proteins in the presence or absence of ATP. Phosphorylation of zFoxj1a and zFoxj1a-T102A was detected by western blot using a phospho-threonine-proline antibody and input proteins were examined by Coomassie blue staining. (I) Ectopical CDK4 expression is unable to stabilize zFoxj1a-T102 mutant. Lysates from HEK293T cells transfected with the indicated plasmids were subjected to immunoblotting.

Figure 7

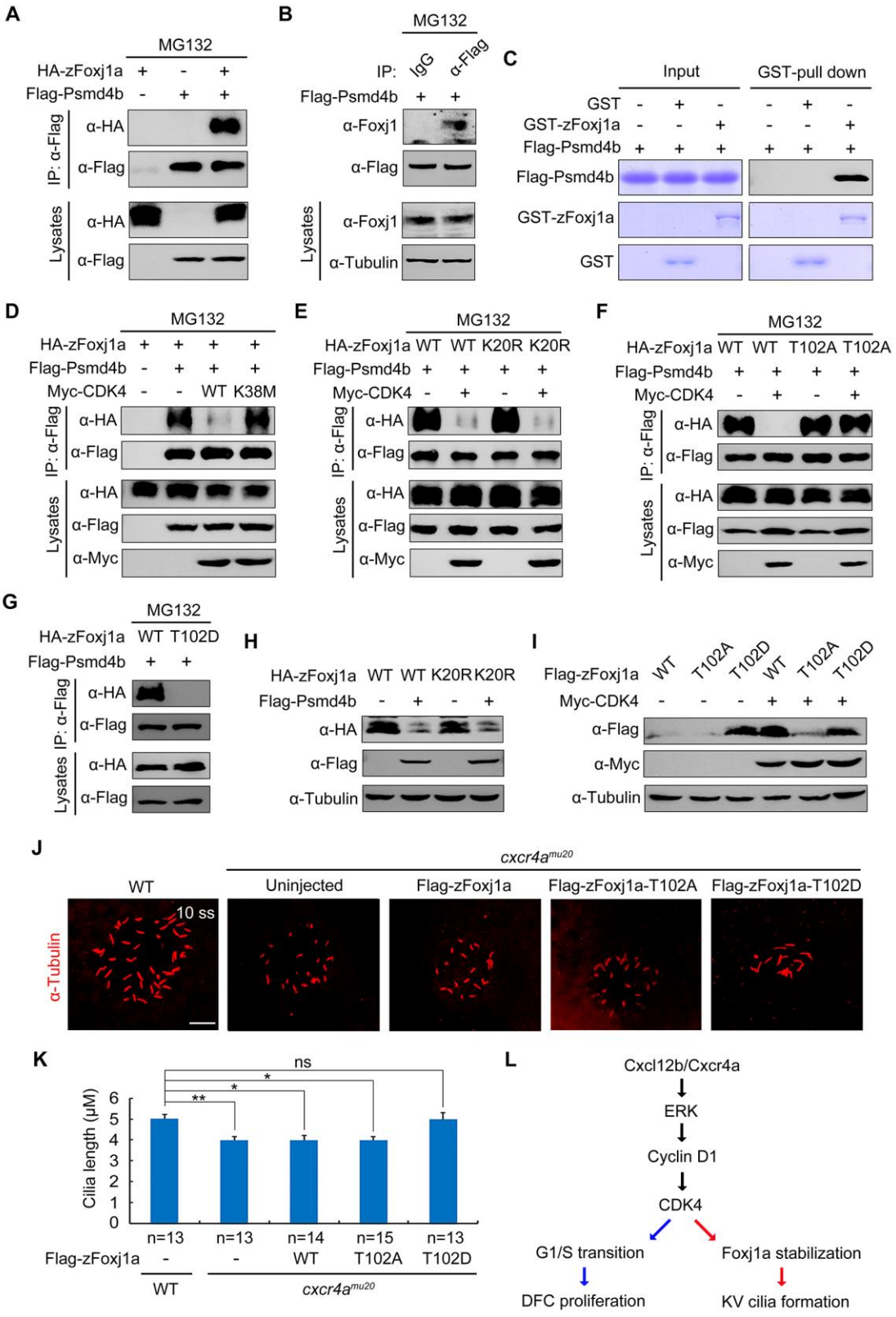

Fig 7. zFoxj1a undergoes Ubiquitin-independent proteasomal degradation via a direct interaction with Psmd4b. (A-B) Flag-Psmd4b interacts with overexpressed or endogenous zFoxj1a. HEK293T cells transfected with the indicated constructs (A) and bud-stage wild-type embryos with DFC-specific expression of Flag-Psmd4b (B) were subjected to immunoprecipitation with the indicated antibodies. (C) *In vitro* GST Pull-Down assays reveal a direct interaction between zFoxj1a and Psmd4b. Purified GST or GST-zFoxj1a proteins were incubated with recombinant Flag-Psmd4b. The presence of Flag-Psmd4b in the protein complex which was pull-downed by Glutathione agarose was assessed by western blot and input proteins were examined by Coomassie blue staining. (D-E) CDK4 kinase activity is required for its inhibitory effect on the association between Psmd4b and zFoxj1a. HEK293T cells transfected with the indicated plasmids were treated with MG132 for 5 hours prior to harvest for immunoprecipitation. Note that ectopically expressed CDK4 efficiently disrupted the association of Psmd4b with zFoxj1a (D) or its lysine-free mutant zFoxj1a-K20R (E), while overexpression of the CDK4 kinase deficient mutant CDK4-K38M had no effect on their interaction (D). (F-G) Psmd4b has a much lower affinity for zFoxj1a-T102D. zFoxj1a-T102A is an unphosphorylated form and zFoxj1a-T102D is a phospho-mimicking mutant of zFoxj1a. Note that Psmd4b was particularly associated with zFoxj1a and zFoxj1a-T102A (F), but was unable to bind zFoxj1a-T102D (G). The association between Psmd4b and zFoxj1a-T102A was unaffected by CDK4 overexpression (F). (H) Psmd4b overexpression induces a dramatic reduction in zFoxj1a expression. Note that a similar reduction in the

expression level of the lysine-free mutant zFoxj1a-K20R was observed upon Psmd4b overexpression. (I) Comparison of protein stability in wild-type zFoxj1a and its mutants. HEK293T cells were transfected with the indicated constructs and harvested for western blot analysis. In comparison to wild-type zFoxj1a and its T102A mutant, the zFoxj1a-T102D mutant exhibited greater stability, but could not be further stabilized by CDK4 overexpression. (J-K) DFC-specific overexpression of zFoxj1a-T102D in *cxcr4a*^{um20} mutants restores KV cilia length. Confocal images of 10-somite-stage *cxcr4a*-deficient embryos were injected with 200 pg of wild-type *zfoxj1a* or *zfoxj1a-T102A* or *zfoxj1a-T102D* mRNA at the 256-cell stage. The resulting embryos were harvested at the 10-somite stage for immunostaining using an antibody against acetylated tubulin (J). Scale bar, 20 μm. Statistical data for cilia length were shown in panel K. Student's *t*-test, **P*<0.05, ***P*<0.01. ns, no significant difference. (L) A schematic diagram showing the regulatory mechanism of Cxcl12/Cxcr4a signaling in DFC proliferation and cilia formation.

1144 **Supporting information**

1145 **Supplemental Figures**

1146 S1 Figure

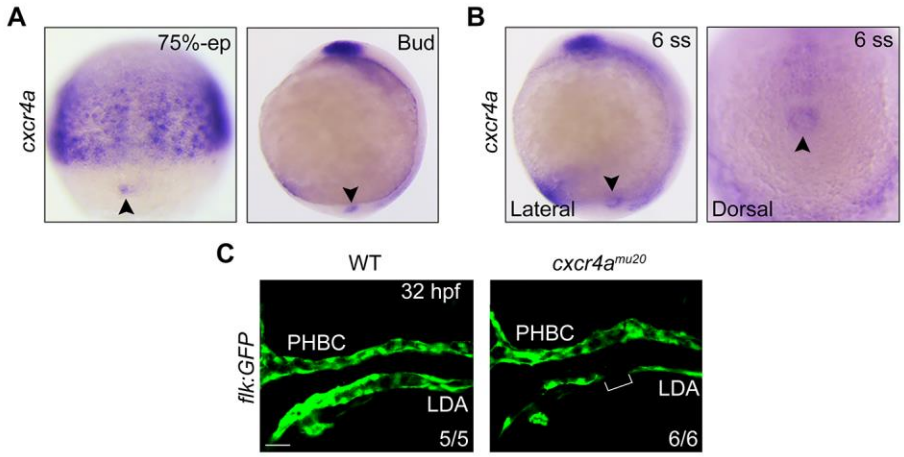

1147

1148 **S1 Fig. The expression of *cxcr4a* in DFCs and KV cells.** (A) *cxcr4a* expression

1149 during gastrulation. *In situ* hybridization of *cxcr4a* in embryos at the 75%-epiboly

1150 stage (Dorsal view with animal pole to the top) and bud stage (Lateral views with

1151 animal pole to the top). Black arrowhead indicates the DFCs.75%-ep, 75%-epiboly.

1152 (B) *cxcr4a* expression at the 6-somite stage. Lateral view was shown with animal pole

1153 to the top in the left panel and dorsal view was shown in the right panel. Black

1154 arrowhead indicates the KV. (C) Confocal images depicting the formation of the

1155 lateral dorsal aorta in live *Tg(flk:GFP)* embryos. Scale bar, 50 μm. LDA, lateral

1156 dorsal aorta; PHBC, primordial hindbrain channel.

1157

1158

1159

1160

1161 S2 Figure

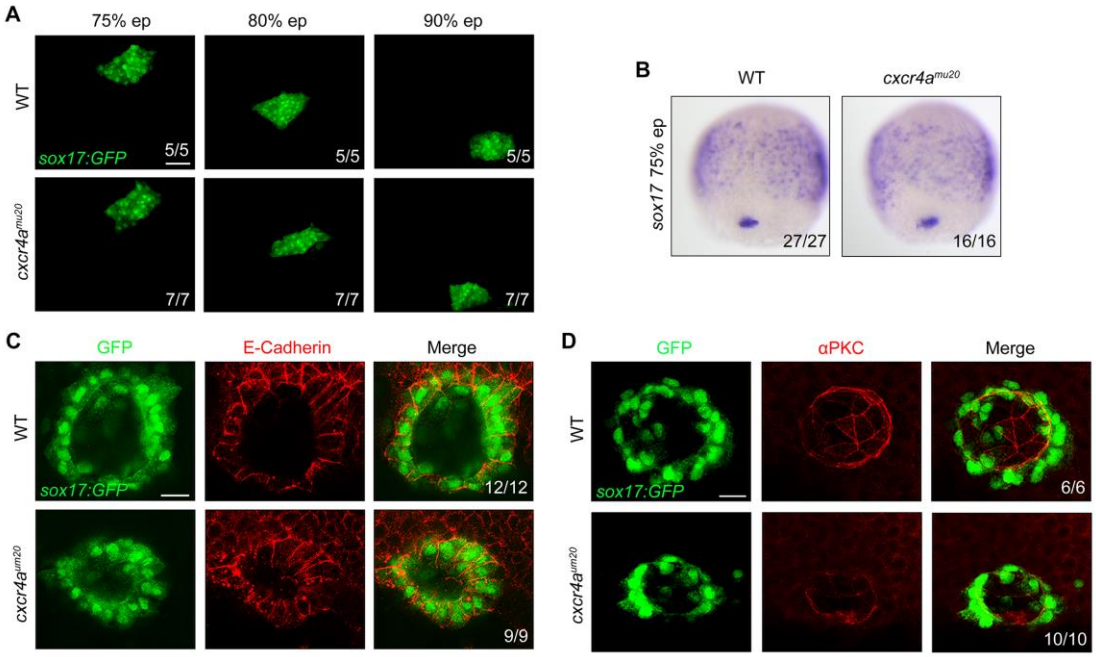

1162

1163 **S2 Fig. *cxcr4a* is unnecessary for the specification, clustering and collective**

1164 **migration of DFCs and dispensable for the polarized differentiation of KV cells.**

1165 (A) Time-lapse confocal images showing DFCs migration in wild-type and *cxcr4a*^{mu20}

1166 mutant embryos on a *Tg(sox17:GFP)* background from 75%- to 90%-eiboly stages.

1167 Scale bar, 50 μm. (B) Sox17 expression was examined by *in situ* hybridization in

1168 wild-type and *cxcr4a*^{mu20} mutants at the 75%-epiboly stage. (C-D) Wild-type and

1169 *cxcr4a*-deficient *Tg(sox17:GFP)* embryos were harvested at the 10-somite stage for

1170 immunostaining. KV cells were labelled using an antibody against GFP (green).

1171 Expression of the basal-lateral marker E-cadherin (C) and the apical marker aPKC (D)

1172 were visualized using the indicated antibodies (red). Scale bar, 20 μm.

1173

1174

1175

S3 Figure

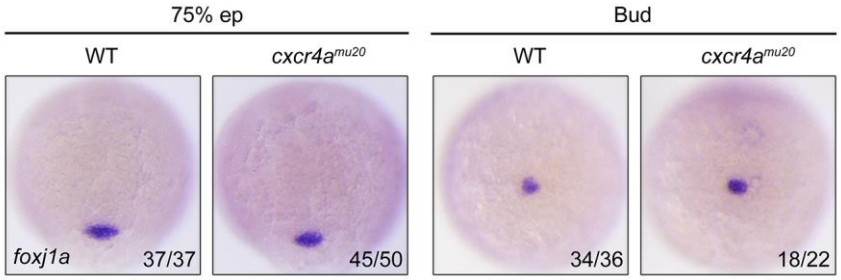

S3 Fig. *cxcr4a*^{mu20} mutants exhibit a normal expression of *cxcr4a* transcripts. *cxcr4a* expression was examined by *in situ* hybridization at the 75%-epiboly and bud stages in wild-type and *cxcr4a*^{mu20} mutant embryos.

1196 S4 Figure

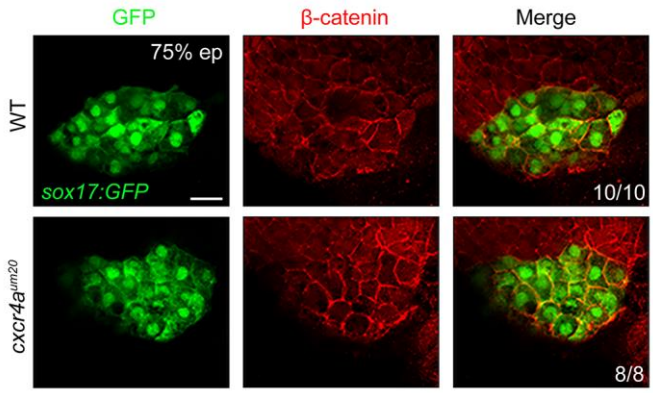

1197

1198 **S4 Fig. Inactivity of *cxcr4a* does not affect β-catenin nuclear accumulation in**

1199 **DFCs.** Wild-type and *cxcr4a*^{mu20} mutants were harvested at the 75%-epiboly stage for

1200 immunofluorescence assays using the indicated antibodies. Scale bar, 20 μm.

1201

1202

1203

1204

1205

1206

1207

1208

1209

1210

1211

1212

1213

1214 S5 Figure

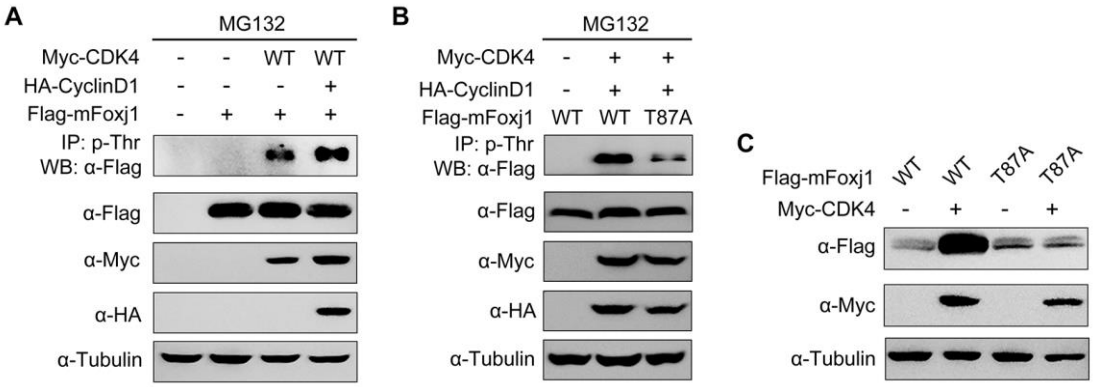

1215

1216 **S5 Fig. CDK4 phosphorylates and stabilizes mFoxj1.** (A-B) HEK293T cells were

1217 transfected with the indicated plasmids and then harvested for immunoprecipitation

1218 with a phospho-threonine-proline antibody. Phosphorylation of mFoxj1 (A) and its

1219 T87A mutant (B) was detected by western blot. Note that the CDK4-mediated

1220 phosphorylation of mFoxj1 was clearly decreased in the T87A mutant. (C) Western

1221 blots of total lysates from HEK293T cells transfected with the indicated plasmids.

1222 Note that CDK4 overexpression could stabilizes wild-type mFoxj1 but not the T87A

1223 mutant.

1224

1225

1226

1227

1228

1229

1230

1231

1232 S6 Figure

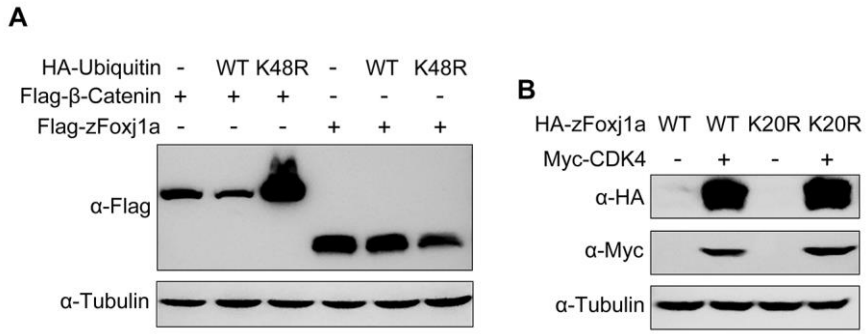

1233

1234 **S6 Fig. Proteasomal degradation of zFoxj1a is independent of ubiquitin**

1235 **modification.** (A) Overexpression of Ub K48R/G76A was unable to stabilize zFoxj1a.

1236 Flag-tagged β-catenin and zFoxj1a were co-expressed with wild-type Ub or Ub

1237 K48R/G76A, a dominant negative inhibitor of chain formation and degradation. Cell

1238 extracts were immunoblotted with the indicated antibodies. (B) CDK4 overexpression

1239 similarly promoted the expression of wild-type zFoxj1a and its lysine-less mutant

1240 K20R.

1241

1242

1243

1244

1245

1246

1247

1248

1249

1250

S7 Figure

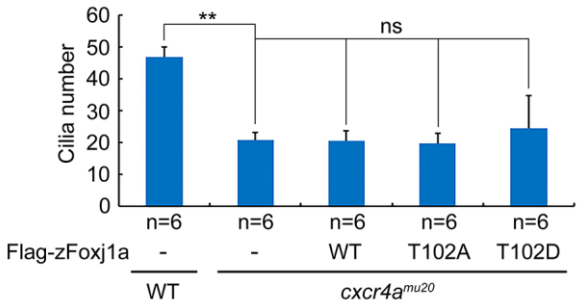

S7 Fig. The decrease in the number of cilia in *cxcr4a*^{um20} mutants was not alleviated by DFC-specific overexpression of wild-type zFoxj1a and its T102A and T102D mutants, respectively. *cxcr4a*-deficient embryos were injected with 200 pg of wild-type *zfoxj1a* or *zfoxj1a-T102A* or *zfoxj1a-T102D* mRNA at the 256-cell stage. The resulting embryos were harvested at the 10-somite stage for immunostaining using an antibody against acetylated tubulin. Cilia length was quantitatively analyzed using ImageJ software. Student's *t*-test, $^{**}P<0.01$. ns, no significant difference.

S1 Video. Wild-type control embryos, normal KV flow. Wild-type *Tg(sox17:GFP)* embryos were injected at the 6-somite stage with fluorescent beads and imaged using a Nikon A1R+ confocal microscope at the 10-somite stage. Dorsal view with anterior to the top.

S2 Video. *cxcr4a*^{mu20} mutant embryos, aberrant KV flow. *cxcr4a*^{mu20} mutant embryos on a *Tg(sox17:GFP)* background were injected at the 6-somite stage with fluorescent beads and imaged using a Nikon A1R+ confocal microscope at the 10-somite stage. Dorsal view with anterior to the top.